P-wave stacking-velocity tomography for VTI media

Vladimir Grechka*, Andres Pech* and Ilya Tsvankin*

(April 22, 2002)

*Center for Wave Phenomena, Department of Geophysics, Colorado School of Mines, Golden, CO 80401-1887

ABSTRACT

A major complication caused by anisotropy in velocity analysis and imaging is the uncertainty in estimating the vertical velocity and depth scale of the model from surface data. For laterally homogeneous VTI (transversely isotropic with a vertical symmetry axis) media above the target reflector, P-wave moveout has to be combined with other information (e.g., borehole data or converted waves) to build velocity models for depth imaging. The presence of lateral heterogeneity in the overburden creates the dependence of P-wave reflection data on all three relevant parameters (the vertical velocity V_{P0} and Thomsen coefficients ϵ and δ) and, therefore, may help to determine the depth scale of the velocity field.

Here, we propose a tomographic algorithm designed to invert NMO ellipses (obtained from azimuthally varying stacking velocities) and zero-offset traveltimes of P-waves for the parameters of homogeneous VTI layers separated by either plane dipping or curved interfaces. For *plane* non-intersecting layer boundaries, the interval parameters cannot be recovered from P-wave moveout in a unique way. Nonetheless, if the reflectors have sufficiently different azimuths, *a priori* knowledge of any single interval parameter makes it possible to reconstruct the whole model in depth. For example, the parameter estimation becomes unique if the subsurface layer is known to be isotropic. In the case of 2-D inversion on the dip line of co-oriented reflectors, it is necessary to specify one parameter (e.g., the vertical velocity) per layer.

Despite the higher complexity of models with *curved* interfaces, the increased angle coverage of reflected rays helps to resolve the trade-offs between the medium parameters. Singular value decomposition (SVD) shows that in the presence of sufficient interface curvature all parameters needed for anisotropic *depth* processing can be obtained solely from conventional-spread P-wave moveout. By performing tests on noise-contaminated data we demonstrate that the tomographic inversion procedure reconstructs both the interfaces and the VTI parameters with high accuracy.

Both SVD analysis and moveout inversion are implemented using an efficient modeling technique based on the theory of NMO-velocity surfaces generalized for wave propagation through curved interfaces.

Keywords.—P-waves, VTI media, moveout inversion, tomography.

INTRODUCTION

Vertical transverse isotropy, believed to be the most common anisotropic model for sedimentary basins, can have a significant influence on velocity analysis and imaging of reflection data. It is well known that the kinematics of P-waves in VTI media is controlled by the vertical velocity V_{P0} and Thomsen's (1986) anisotropic coefficients ϵ and δ (for a detailed overview, see Tsvankin 2001). Accurate estimation of these parameters from reflection data is a key issue in building VTI velocity models for seismic imaging.

Inversion of P-wave data in VTI media was addressed in a number of recent publications, including Bube and Meadows (1997), Grechka and Tsvankin (1998), Bartel et al. (1998), Le Stunff and Grenié (1998), Le Stunff and Jeannot (1998) and Sexton and Williamson (1998). Time-domain imaging for vertical transverse isotropy is largely based on the result of Alkhalifah and Tsvankin (1995) who proved that P-wave moveout for *laterally homogeneous* VTI media above the reflector depends on just two parameters – the normal-moveout (NMO) velocity from a horizontal (zero-dip) reflector $V_{\rm nmo}(0)$ and the anellipticity coefficient η:

$$V_{\rm nmo}(0) = V_{P0}\,\sqrt{1+2\,\delta}\,, \tag{1}$$

and

$$\eta \equiv \frac{\epsilon-\delta}{1+2\,\delta}\,. \tag{2}$$

Whereas $V_{\rm nmo}(0)$ and η are sufficient to carry out time processing [i.e., NMO correction, DMO (dip-moveout) removal and time migration], they do not constrain the

vertical velocity V_{P0} and reflector depth – parameters needed for anisotropic depth imaging.

The two-parameter description of P-wave time-domain signatures, however, breaks down in the presence of *lateral heterogeneity* above the reflector (Alkhalifah, Biondi and Fomel 1998; Grechka and Tsvankin 1999b). Although lateral velocity variations or non-horizontal interfaces introduce additional unknowns to be estimated from reflection data, they may also provide information about the Thomsen parameters. Grechka and Tsvankin (1999b) developed a Dix-type averaging procedure for NMO velocities in laterally heterogeneous anisotropic media and applied it to moveout analysis for vertical transverse isotropy. Their results show that the NMO velocity of reflected P-wave arrivals which cross dipping intermediate interfaces depends on the individual values of V_{P0}, ϵ and δ. Le Stunff, Grechka and Tsvankin (2001) presented an example of a successful inversion of P-wave traveltimes for the parameters V_{P0}, ϵ and δ of a dipping VTI layer overlying a homogeneous isotropic medium.

The topic of this paper is P-wave moveout inversion for more complicated VTI models composed of multiple homogeneous layers separated by either plane dipping or curved interfaces. Our analysis demonstrates that 3-D wide-azimuth P-wave moveout data from N *plane* non-intersecting interfaces constrain up to $3N-1$ combinations of the $3N$ interval parameters $V_{P0,n}$, ϵ_n, δ_n $(n = 1, \ldots, N)$. Hence, to determine the interval values $V_{P0,n}$, ϵ_n, and δ_n uniquely and reconstruct the model in depth, at least one of the parameters has to be known *a priori*. The inversion is generally better posed if the subsurface contains additional reflecting boundaries, such as fault planes.

To carry out parameter estimation for VTI media with *curved* boundaries, we develop an efficient algorithm for modeling multi-azimuth and multi-offset reflection traveltimes based on an extension of the theory of NMO-velocity surfaces (Grechka and Tsvankin 1999b). Singular value decomposition and actual inversion of P-wave reflection data show that for some VTI models with smooth curved interfaces parameter estimation in depth can be accomplished without any *a priori* information.

MODELS WITH PLANE DIPPING INTERFACES

Methodology of tomographic inversion

Model representation and input data.—We consider a model composed of N homogeneous VTI layers (some of them may be isotropic) separated by plane dipping non-intersecting interfaces (Fig. 1). The inversion methodology introduced here operates exclusively with surface P-wave data acquired in wide-azimuth 3-D surveys. The model parameters responsible for P-wave kinematics include the interval vertical velocities $V_{P0,n}$, anisotropic coefficients ϵ_n and δ_n, and the interface dips ϕ_n, azimuths ψ_n and depths z_n (the depth can be measured, for example, under the coordinate origin $\mathbf{O}$). Thus, the model vector

$$\mathbf{m} \equiv \{V_{P0,n},\, \epsilon_n,\, \delta_n,\, \phi_n,\, \psi_n,\, z_n\}\,, \quad (n = 1,\, \ldots,\, N) \tag{3}$$

is characterized by $6N$ independent quantities. It is convenient to split the vector $\mathbf{m}$ into two vectors $\mathbf{l}$ and $\mathbf{i}$, where $\mathbf{l}$ contains the layer parameters,

$$\mathbf{l} \equiv \{V_{P0,n},\, \epsilon_n,\, \delta_n\}\,, \quad (n = 1,\, \ldots,\, N)\,, \tag{4}$$

and $\mathbf{i}$ describes the interfaces,

$$\mathbf{i} \equiv \{\phi_n,\, \psi_n,\, z_n\}\,, \quad (n = 1,\, \ldots,\, N)\,. \tag{5}$$

Clearly, each vector ($\mathbf{l}$ and $\mathbf{i}$) has $3N$ components.

Velocity analysis of 3-D multi-azimuth P-wave data recorded at common midpoints (CMP) with coordinates $\mathbf{Y} = [Y_1,\, Y_2]$ can provide the one-way zero-offset reflection traveltimes $\tau_0(\mathbf{Y},\, n)$ from all interfaces and the corresponding NMO velocities $V_{\rm nmo}(\alpha)$ (α is the azimuth). Azimuthally dependent NMO velocity of any pure mode is described by an ellipse that can be expressed in terms of a 2×2 symmetric matrix $\mathbf{W}$ (Grechka and Tsvankin 1998):

$$V_{\rm nmo}^{-2}(\alpha) = W_{11} \cos^2 \alpha + 2\, W_{12} \sin\alpha \cos\alpha + W_{22} \sin^2 \alpha\,, \tag{6}$$

where

$$W_{ij} = \tau_0 \left. \frac{\partial^2 \tau}{\partial x_i \partial x_j} \right|_{\mathbf{x}=\mathbf{Y}} = \tau_0 \left. \frac{\partial p_i}{\partial x_j} \right|_{\mathbf{x}=\mathbf{Y}}, \qquad (i, j = 1, 2)\,. \tag{7}$$

Here $\tau(x_1,\, x_2)$ is the one-way traveltime from the zero-offset reflection point to the location $\mathbf{x}\,\{x_1,\, x_2\}$ at the surface, τ_0 is the one-way zero-offset traveltime, and p_i are the components of the slowness vector corresponding to the ray recorded at the point $\mathbf{x}$.

The matrices $\mathbf{W}(\mathbf{Y},\, n)$ can be obtained from azimuthal velocity analysis based on the hyperbolic moveout equation parameterized by the NMO ellipse, as described by Grechka and Tsvankin (1999a). Using the zero-offset (or stacked) time sections of reflection events, we can pick the reflection slopes and determine the ray parameters $\mathbf{p}(\mathbf{Y},\, n) = [p_1(\mathbf{Y},\, n),\, p_2(\mathbf{Y},\, n)]$ of the zero-offset rays.

Since the layers in our model are homogeneous and the interfaces are plane (Fig. 1), the slowness components $p_1(\mathbf{Y},\, n)$, $p_2(\mathbf{Y},\, n)$ are independent of the CMP coordinate $\mathbf{Y}$. Taking into account that

$$\frac{\partial \tau_0(\mathbf{Y},\, n)}{\partial Y_j} = p_j(n)\,, \quad (j = 1, 2)\,, \tag{8}$$

the traveltimes $\tau_0(\mathbf{Y},\, n)$ can be expressed as *linear* functions of Y_j:

$$\tau_0(\mathbf{Y},\, n) = \tau_0(\mathbf{O},\, n) + p_1(n)\, Y_1 + p_2(n)\, Y_2\,. \tag{9}$$

Here $\tau_0(\mathbf{O},\, n)$ are the traveltimes recorded at the coordinate origin $\mathbf{O}$. Using equation (9), the input data $\mathbf{d}(\mathbf{Y},\, n)$ can thus be represented in the following form:

$$\mathbf{d}(\mathbf{Y},\, n) \equiv \{\tau_0(\mathbf{O},\, n),\, p_1(n),\, p_2(n),\, W_{11}(\mathbf{Y},\, n),\, W_{12}(\mathbf{Y},\, n),\, W_{22}(\mathbf{Y},\, n)\}\,, \tag{10}$$

where $n = 1,\, \ldots,\, N$.

The feasibility of the inversion for $\mathbf{m}$ is controlled by the character of the spatial variation of the effective NMO ellipses $\mathbf{W}(\mathbf{Y},\, n)$. To analyze the dependence of $\mathbf{W}$ on the CMP coordinate $\mathbf{Y}$, we next review the procedure of building effective NMO ellipses in laterally heterogeneous media.

Effective NMO ellipse.—Grechka and Tsvankin (1999b) introduced the concept of *NMO-velocity surfaces* and used it to develop a methodology for obtaining effective (i.e., measured at the surface) NMO ellipses $\mathbf{W}$ in laterally heterogeneous anisotropic media. Two relevant results of their work applicable to the model at hand are summarized below.

The NMO-velocity $V_{\rm nmo}(\mathcal{L})$ recorded along CMP line $\mathcal{L}$ arbitrarily oriented in 3-D space is given by

$$\frac{1}{V^2_{\rm nmo}(\mathcal{L})} = \mathcal{L}\,\mathbf{U}\,\mathcal{L}^{\mathbf{T}}\,, \tag{11}$$

where $\mathcal{L}$ is the unit vector and $\mathbf{T}$ denotes transposition. The 3×3 symmetric matrix $\mathbf{U}$ is expressed in terms of the spatial derivatives of the one-way traveltime τ or the slowness vector $\mathbf{p}$:

$$U_{km} = \tau_0\,\left.\frac{\partial^2\tau(\mathbf{x})}{\partial x_k\,\partial x_m}\right|_{\mathbf{x}=\mathbf{Y}} = \tau_0\,\left.\frac{\partial p_k(\mathbf{x})}{\partial x_m}\right|_{\mathbf{x}=\mathbf{Y}}, \qquad (k,m=1,2,3)\,. \tag{12}$$

Here τ_0 is the one-way zero-offset traveltime, and the derivatives are evaluated at the CMP location $\mathbf{x}=\mathbf{Y}$.

The matrix $\mathbf{U}$ describes a quadratic *NMO-velocity surface* obtained by plotting NMO velocity as the radius-vector along all possible directions of CMP lines. Grechka and Tsvankin (1999b) showed that if the medium in the vicinity of the common midpoint is homogeneous, then

$$\det\mathbf{U} = 0\,, \tag{13}$$

and the NMO-velocity surface is a cylinder. Other possible shapes include an ellipsoid and a one-sheeted hyperboloid. The NMO ellipse $\mathbf{W}$ recorded in the plane $\mathcal{P}$ can be viewed as the intersection of the NMO-velocity surface $\mathbf{U}$ with $\mathcal{P}$:

$$\mathbf{W} = \mathbf{U}\bigcap\mathcal{P}\,. \tag{14}$$

In particular, if $\mathcal{P}$ is a horizontal plane, equation (14) defines the NMO ellipse (7).

The Dix-type averaging procedure of Grechka, Tsvankin and Cohen (1999) is applicable to the *intersections* $\mathbf{W}_n(\mathbf{Y})$ of the interval NMO-velocity cylinders (see Grechka and Tsvankin 1999b) by the model interfaces. Each interval cylinder is computed for a fictitious reflector orthogonal to the slowness vector of the interval zero-offset ray. For example, suppose the model contains two layers separated by a dipping interface (Fig. 2). Then the intersection $\bar{\mathbf{W}}(\mathbf{Y},\, 2)$ of the effective NMO-velocity cylinder (measured at the surface) with a plane parallel to the intermediate interface is obtained from the following Dix-type averaging formula:

$$\tau_0(\mathbf{Y},\, 2)\, \left[\bar{\mathbf{W}}(\mathbf{Y},\, 2)\right]^{-1} = \tau_{0,1}(\mathbf{Y})\, \left[\mathbf{W}_1(\mathbf{Y})\right]^{-1} + \tau_{0,2}(\mathbf{Y})\, \left[\mathbf{W}_2(\mathbf{Y})\right]^{-1}\,, \tag{15}$$

where $\tau_{0,1}$ and $\tau_{0,2}$ are the interval zero-offset traveltimes, $\mathbf{W}_1(\mathbf{Y})$ (shaded in gray) and $\mathbf{W}_2(\mathbf{Y})$ (dashed) are the intersections of the NMO-velocity cylinders in the first and second layers with the intermediate interface. The ellipse described by $\bar{\mathbf{W}}(\mathbf{Y},\, 2)$ is then projected along the effective NMO-velocity cylinder onto the horizontal plane to find the effective NMO ellipse $\mathbf{W}(\mathbf{Y},\, 2)$.

In the model with plane interfaces (Fig. 1), zero-offset ray trajectories from the same interface are parallel to each other at different CMP locations $\mathbf{Y}$. As a result, the interval slownesses, group-velocity vectors and the matrices $\mathbf{W}_n$ [equation (15)] are independent of the CMP coordinate $\mathbf{Y}$, whereas the interval traveltimes $\tau_{0,n}(\mathbf{Y})$ are *linear* functions of $\mathbf{Y}$. Therefore, the NMO ellipses $\mathbf{W}(\mathbf{O},\, n)$ and $\mathbf{W}(\mathbf{Y},\, n)$ measured at points $\mathbf{O}$ and $\mathbf{Y}$ differ only due to variations in the length of the interval ray segments. This suggests that the dependence of $\mathbf{W}(\mathbf{Y},\, n)$ on $\mathbf{Y}$ does not provide any information about the model parameters not contained in the NMO ellipses $\mathbf{W}(\mathbf{O},\, n)$. The conclusion that it is sufficient to measure the NMO ellipses at a single CMP location is supported by numerical results below.

Thus, the data vector (10) can be written as

$$\mathbf{d}(\mathbf{Y},\, n) = \{\mathbf{d}(\mathbf{O},\, n),\, \mathbf{Y} - \mathbf{O}\}\,. \tag{16}$$

Feasibility of parameter estimation

It is clear from equation (16) that although traveltime data at different common midpoints may be useful in practice to suppress noise, they give the same information about the medium parameters as does the data vector

$$\mathbf{d}(\mathbf{O},\, n) = \{\tau_0(\mathbf{O},\, n),\, \mathbf{p}(n),\, \mathbf{W}(\mathbf{O},\, n)\} \tag{17}$$

at a single CMP. Thus, analyzing the dependence of the vector $\mathbf{d}(\mathbf{O},\, n)$ on the parameter vector $\mathbf{m}$ [equation (3)] should be sufficient for evaluating the feasibility of the inversion. For brevity, henceforth the CMP coordinate will be omitted.

For an N-layered VTI model, the vectors $\mathbf{d}$ and $\mathbf{m}$ contain $6N$ components each. Therefore, the vector $\mathbf{m}$ can be obtained uniquely from the data $\mathbf{d}$ only if all components of $\mathbf{d}$ are independent. Unfortunately, this is not the case for VTI media. The P-wave NMO ellipse $\mathbf{W}(1)$ from a dipping reflector overlaid by a homogeneous VTI medium provides only two equations for the medium parameters because its orientation is fixed by the reflector azimuth ψ_1 that can be found from the reflection slopes (Grechka and Tsvankin 1998):

$$\tan\psi_1 = \frac{p_2(1)}{p_1(1)} = \frac{W_{22}(1) - W_{11}(1) + \sqrt{[W_{22}(1) - W_{11}(1)]^2 + 4\,W_{12}^2(1)}}{2\,W_{12}(1)}\,. \tag{18}$$

Specifically, the semi-axes of the NMO ellipse in the first layer constrain the zero-dip NMO velocity $V_{\rm nmo}(0)$ and the anellipticity coefficient η [equations (1) and (2)]. As a result, the data vector in the top layer contains only five components. Singular-value decomposition (SVD) analysis performed below shows that if all interfaces have different strikes, this is the *only* relationship among the components of the data vector.

For inversion purposes, it is convenient to split the vector $\mathbf{d}(\mathbf{O},\, n)$ into two parts. For a given ("trial") set of the interval VTI parameters $\tilde{\mathbf{l}}_n$ [equation (4)], the values of $\tau_0(n)$ and the horizontal slownesses $p_1(n)$, $p_2(n)$ can be used to estimate the depths,

dips and azimuths of the interfaces $\tilde{\mathbf{i}}_n$ [equation (5)]. Indeed, knowledge of the parameters of the first layer $\tilde{\mathbf{l}}_1$ is sufficient for computing the vertical slowness component from the Christoffel equation and obtaining the slowness vector $[\,p_1(1),\, p_2(1),\, p_3(1)\,]$. Since the slowness vector of the zero-offset ray is orthogonal to the reflector, it defines the reflector normal. Then we can find the group-velocity vector (ray) in the first layer and use the traveltime $\tau_0(1)$ to determine the depth z_1 of the first reflector.

Once the first interface has been reconstructed, the slowness vector in the second layer can be obtained from Snell's law and used to find the orientation of the second reflector. The zero-offset traveltime of the reflection from the second interface gives an estimate of the reflector depth, etc. Continuing this procedure downward yields the dips, strikes (or azimuths) and depths of all interfaces of the trial model. Evidently, any errors in the input data or trial layer parameters $\tilde{\mathbf{l}}_n$ will distort the interfaces $\tilde{\mathbf{i}}_n$.

The best-fit vector of the layer parameters $\mathbf{l}_n$ has to be found by inverting the NMO ellipses $\mathbf{W}(n)$ because the rest of the input data was already used to reconstruct the interfaces. Therefore, to study the feasibility of the inversion procedure it is sufficient to perform SVD analysis of the $3N \times 3N$ matrix of Frechét derivatives

$$\mathcal{F} = \frac{\partial\, \mathbf{W}(n)}{\partial\, \mathbf{l}_k}\,, \quad (k, n = 1,\, \ldots,\, N)\,. \tag{19}$$

Here we assume that the vector $\mathbf{i}$, which specifies the interfaces, is such that the zero-offset traveltimes and horizontal slowness components for each trial model exactly match those in the data. The NMO ellipses are computed using the formalism developed by Grechka and Tsvankin (1999b).

Figure 3 shows a typical result of SVD analysis of the NMO ellipses for the parameters $\mathbf{l} = \{V_{P0,1},\, \epsilon_1,\, \delta_1,\, V_{P0,2},\, \epsilon_2,\, \delta_2\}$ in a two-layer model. While the last singular value is always equal to zero, the other five do not vanish if the azimuths of the interfaces are different (see the curves marked by squares, diamonds and triangles). The presence of two vanishing singular values when the strikes of both interfaces coincide (the circles in Fig. 3) is not surprising, because in this case the axes of the NMO

ellipse from the bottom of the model are aligned with the dip and strike directions (i.e., the model becomes 2-D), and there is one less independent data component.

The model from Fig. 3 can be used to support the statement that the inversion results are independent of the CMP location. We repeated our computation for a number of different common midpoints and obtained the same curves of singular values as those in Fig. 3. Moreover, the singular values do not change when the NMO ellipses computed at a number of CMP locations are used in the Frechét matrix (19) *simultaneously*. Therefore, it is indeed sufficient to carry out the inversion using the NMO ellipses from all interfaces measured at a single CMP.

To get a more quantitative assessment of the feasibility of the inversion for the model from Fig. 3, we performed a series of SVD analyses of the matrix W_{ij} for different values of the dip (ϕ_1) and azimuth (ψ_1) of the first interface. The results, displayed in Fig. 4, indicate that it should be possible to estimate five parameter combinations for any ϕ_1 and ψ_1, except for $\phi_1 = 0^\circ$ and $\psi_1 = 0^\circ$ or 180°. In the first case ($\phi_1 = 0^\circ$), the first layer is horizontal and the NMO ellipse $W(1)$ degenerates into a circle that constrains just one combination of the medium parameters. For $\psi_1 = 0^\circ$ or 180°, the two reflectors are co-oriented, and the 3-D model becomes 2-D, which reduces the number of equations to four.

The observations drawn from Figs 3 and 4 can be extended to an arbitrary number of VTI layers. At a maximum, the NMO ellipses constrain $3N - 1$ combinations of the $3N$ interval parameters $\{V_{P0,n},\, \epsilon_n,\, \delta_n\}$ $(n = 1,\, \ldots,\, N)$, provided the model interfaces have different azimuths. Otherwise, P-wave traveltimes contain less information about the medium. For instance, if the azimuths of all interfaces are identical, the model degenerates into 2-D, and the NMO ellipses from different reflectors are co-oriented. Thus, only their semi-axes constrain the layer parameters, and the number of independent equations reduces to $2N$. In the limiting case of horizontal layers, the NMO ellipses become circles defined by the N interval zero-dip NMO velocities [equation (1)]. Hence, unambiguous inversion is impossible without additional information;

some practical possibilities are discussed below.

Parameter estimation using *a priori* information

Specifying one of the parameters.—The results of the previous section suggest that *a priori* knowledge of a single layer parameter may be sufficient to overcome the ambiguity. For example, it might be possible to estimate the vertical velocity $V_{P0,1}$ in the top layer using a shallow borehole and then obtain the anisotropic parameters ϵ_1 and δ_1 from the NMO ellipse $\mathbf{W}(1)$. According to our SVD results, this should be sufficient for estimating the remaining medium parameters.

To verify this conclusion, we performed several numerical tests, with typical results listed in Table 1. We traced reflected rays through a three-layer VTI model for nine CMP locations (Fig. 5 and Table 1), added Gaussian noise to the computed NMO velocities and zero-offset traveltimes, and found the layer parameters by least-squares fitting of the NMO ellipses. Although, as discussed above, multiple common midpoints do not provide new information for the inversion, they help to obtain more stable results in the presence of random noise.

To constrain the inversion, the parameter $\delta_1 = 0.04$ was assumed to be known, which allowed the other parameters to be estimated with good accuracy (Table 1). The errors generally increase with depth, as can be expected from Dix-type algorithms. The low accuracy in the parameter ϵ_3 in the bottom layer is also associated with insufficient angle coverage of the reflected rays.

The choice of δ_1 as the known parameter was arbitrary; holding any other interval parameter at the correct value produces similar results. It is always possible to reconstruct the whole model if the vertical velocity $V_{P0,n}$ or one of the anisotropic coefficients (ϵ_n or δ_n) in any layer is known. The inversion procedure also works well in the special case of isotropy, i.e., when ϵ_n and δ_n are set to zero in one or more layers.

Specifying vertical velocity in 2-D models.—We also examined the case when all interfaces in the three-layer medium discussed above have the same azimuth. The axes of the NMO ellipses W(1), W(2), and W(3) in such a model are parallel to the dip and strike directions, and the moveout data provide only six equations (two semi-axes for each ellipse). Since the model has a total of nine medium parameters (three per layer), three parameters have to be specified in advance.

One possibility, examined in the test from Fig. 6 and Table 2, is to assume that the vertical velocities in the model are known, for example, from vertical seismic profiling (VSP) data. We modeled the NMO ellipses and zero-offset traveltimes for several CMP locations distributed along the dip direction (Fig. 6) and performed the inversion of noise-contaminated data. The vertical velocities in each layer, $V_{P0,1} = 1$ km/s, $V_{P0,2} = 2$ km/s, and $V_{P0,3} = 3$ km/s, were assumed to be known. The inverted interval parameters ϵ_n and δ_n are in close agreement with the actual values (Table 2). Comparable accuracy was achieved in a number of other tests involving more layers and different levels of noise.

Specifying a relationship between ϵ and δ.—Another way to reduce the number of unknowns is to impose an empirical relationship between ϵ and δ, such as those discussed by Ryan-Grigor (1998), in at least one layer. We found that making ϵ a known function of δ [i.e., $\epsilon = \epsilon(\delta)$] generally makes the parameter estimation unique.

Let us assume, for example, that the relationship between the interval ϵ_n and δ_n is linear ($\delta_n = k_n\,\epsilon_n$), with the coefficients k_n known *a priori*. Figure 7 displays the contours of the smallest singular value for a two-layer VTI model in which $\delta_1 = k_1\,\epsilon_1$ and $\delta_2 = k_2\,\epsilon_2$ (in principle, specifying k_1 alone would be sufficient). Although this singular value was computed as a function of k_1 and k_2, the axes in Fig. 7 are labeled in terms of the anellipticity coefficients $\eta_n \equiv (\epsilon_n - \delta_n)/(1 + 2\,\delta_n)$ (for weak anisotropy, $\eta_n \approx \epsilon_n - \delta_n$) to demonstrate that the only vanishing singular value corresponds to elliptical anisotropy of the whole model (i.e., $\eta_1 = \eta_2 = 0$). If either $\eta_1 \neq 0$ or $\eta_2 \neq 0$,

none of the eigenvalues goes to zero, and the inversion becomes feasible. This is illustrated by the satisfactory inversion results for the model with $\eta_1 = \eta_2 = 0.05$ in Table 3.

One special case when this approach does not help is elliptical anisotropy. Even if all layers are known to be elliptically anisotropic ($k_n = 1$, $\epsilon_n = \delta_n$), and the number of the relevant VTI parameters reduces to $2N$, the $3N - 1$ equations for the NMO ellipses do not have a unique solution. This conclusion is in agreement with the results of Dellinger and Muir (1988) obtained using linear transformations (stretching) of the isotropic wave equation.

Models with intersecting boundaries

A priori information may not be needed at all for models with intersecting boundaries in some of the layers. The presence of different reflector dips in the same depth interval causes reflected rays to span more spatial directions, which helps to constrain the interval anisotropic parameters. While media with curved interfaces are discussed in detail in the next section, here we show how additional dips can remove the nonuniqueness in the parameter estimation.

Let us suppose, for example, that the intermediate interface in the two-layer VTI model from Fig. 3 is bent in such a way that it has two plane portions with the same dip $\phi_1 = 40^\circ$ but different azimuths $\psi_1 = 30^\circ$ and $\psi_1 = 90^\circ$. Recording reflections from the bottom of the model that cross both portions of the intermediate interface yields an additional NMO ellipse (i.e., three more equations). The absence of vanishing singular values for this problem (Fig. 8; the smallest singular value is 0.02) indicates that all parameters can be resolved uniquely.

Parameter estimation may also become feasible if the model contains a dipping fault plane, and the data include the reflections from both the fault and layer boundaries. A similar model was used by Alkhalifah and Tsvankin (1995), who developed

a dip-moveout inversion method to estimate the interval values of η from surface P-wave data. Alkhalifah and Tsvankin (1995), however, assumed that each zero-offset reflected ray crosses only *horizontal* interfaces on its way to the surface.

In our models (e.g., Fig. 9), intermediate interfaces are dipping, which creates the dependence of NMO ellipses from both horizontal and dipping reflectors on the interval values of ϵ and δ. Even for 2-D media, fault planes in some of the layers may make it possible to determine all relevant VTI parameters. For example, the semi-axes of the three NMO ellipses corresponding to the zero-offset rays marked in Fig. 9 provide us with six equations. SVD analysis reveals no zero singular values (i.e., the interval parameters can be found uniquely), albeit the smallest singular value in this case is just 0.0014 compared to 0.02 in Fig. 8.

MODELS WITH CURVED INTERFACES

Here the tomographic methodology is extended to wide-azimuth P-wave data acquired over layered VTI media with curved interfaces. First, we develop an efficient moveout modeling algorithm by introducing a correction for the interface curvature into the Dix-type equations of Grechka and Tsvankin (1999b).

NMO velocity in anisotropic media with curved interfaces

NMO velocity on a curved CMP line.—If the CMP line $\boldsymbol{\sigma}$ is curved, as in acquisition from non-flat topography (e.g., Gray, Maclean and Marfurt 1999), its curvature will influence the value of NMO velocity $V_{\rm nmo}(\boldsymbol{\sigma})$. The expression for $V_{\rm nmo}(\boldsymbol{\sigma})$ is derived in Appendix A:

$$V_{\rm nmo}^{-2}(\boldsymbol{\sigma}) = \boldsymbol{\mathcal{L}}\,\mathbf{U}\,\boldsymbol{\mathcal{L}}^{\mathbf{T}} + \tau_0\,\mathbf{p}\cdot\boldsymbol{\mathcal{K}}\,, \tag{20}$$

where

$$\mathcal{K} = \left. \frac{d^2\boldsymbol{\sigma}(h)}{dh^2} \right|_{h=0} \tag{21}$$

is the second-order derivative of the radius-vector $\boldsymbol{\sigma}$ with respect to the half-offset h; it is evaluated at the common midpoint (zero offset). Depending on the sign of the dot product $\mathbf{p} \cdot \mathcal{K}$, the line curvature can either increase or reduce the NMO velocity.

Dix-type averaging in media with curved interfaces.—Equation (20) can be applied to a CMP line $\boldsymbol{\sigma}$ confined to any curved surface $\mathbf{s}$. The NMO velocity $V_{\rm nmo}(\mathbf{s}, \ell)$ along direction ℓ on $\mathbf{s}$ is given by equation (B-9),

$$V_{\rm nmo}^{-2}(\mathbf{s}, \ell) = \ell \, (\mathbf{W} + \tau_0 \, \mathbf{p} \cdot \boldsymbol{\kappa}) \, \ell^{\mathbf{T}} , \tag{22}$$

where $\mathbf{W}$ is the NMO ellipse obtained as the intersection of the NMO-velocity surface $\mathbf{U}$ with the plane $\mathcal{P}$ tangent to $\mathbf{s}$ at the common midpoint. The matrix

$$\boldsymbol{\kappa}_{ij} = \left. \frac{\partial^2 \mathbf{s}}{\partial h_i \, \partial h_j} \right|_{h_1 = h_2 = 0} , \quad (i, j = 1, 2) \tag{23}$$

is composed of the second-order derivatives of $\mathbf{s}(h_1, \, h_2)$ with respect to the half-offsets h_1 and h_2 (Fig. B-1); the values $h_1 = h_2 = 0$ correspond to the CMP location.

If $\mathbf{s}$ represents the boundary between two layers, the NMO ellipse is discontinuous across the tangent plane $\mathcal{P}$, with the jump depending on the difference between the slowness vectors above ($\mathbf{p}^{(+)}$) and below ($\mathbf{p}^{(-)}$) surface $\mathbf{s}$. As shown in Appendix C, equation (22) leads to the following expression for the NMO ellipse $\mathbf{W}^{(+)}$ on the "positive" side of the interface:

$$\mathbf{W}^{(+)} = \mathbf{W}^{(-)} - \tau_0 \, \left(\mathbf{p}^{(+)} - \mathbf{p}^{(-)} \right) \cdot \boldsymbol{\kappa} , \tag{24}$$

where the term $\tau_0 \left(\mathbf{p}^{(+)} - \mathbf{p}^{(-)} \right) \cdot \boldsymbol{\kappa}$ represents a correction for the interface curvature.

The above results make it possible to generalize the Dix-type averaging procedure of Grechka and Tsvankin (1999b) to media with curved interfaces. Suppose the model above the reflector contains N homogeneous layers, and we obtained the NMO-velocity cylinder in the layer immediately above the reflector. Slicing this cylinder by

the plane tangent to the $N-1$th interface at the intersection point of the zero-offset ray yields the NMO ellipse $\mathbf{W}_{n-1}^{(-)}$. Applying equation (24), we find the ellipse $\mathbf{W}_{n-1}^{(+)}$ corrected for the interface curvature. Then this procedure continues upward, and the results are substituted into the Dix-type averaging equation:

$$[\mathbf{W}(N)]^{-1} \sum_{n=1}^{N} \tau_{0,n} = \sum_{n=1}^{N} \left[\mathbf{W}_n^{(+)}\right]^{-1} \tau_{0,n}\,, \tag{25}$$

where $\mathbf{W}(N)$ is the effective NMO ellipse at the earth's surface, and $\tau_{0,n}$ are the interval zero-offset traveltimes. Application of equation (25) involves projecting the NMO-velocity cylinders onto the planes tangent to the layer interfaces following the methodology of Grechka and Tsvankin (1999b). Note that equation (15) introduced above is a special case of equation (25) for a two-layer model with a plane intermediate interface.

Equation (25) allows us to compute the effective NMO ellipse $\mathbf{W}$, which can be obtained from velocity analysis of 3-D multi-azimuth reflection data. Since it is necessary to trace only one (zero-offset) ray per common midpoint, the hyperbolic portion of pure-mode reflection moveout can be modeled without the time-consuming calculation of multi-offset and multi-azimuth traveltimes.

Methodology of inversion

Model representation and input data.—The above theory provides a convenient tool for traveltime modeling that can be efficiently used in parameter-estimation algorithms. As before, the input data $\mathbf{d}$ include the NMO ellipses $\mathbf{W}(n)$, the zero-offset P-wave traveltimes $\tau_0(n)$, and the reflection slopes in orthogonal directions (horizontal slownesses) $\mathbf{p}(n) = [p_1(n),\, p_2(n)]$ measured for all interfaces ($n = 1,\, \ldots,\, N$). This set of input parameters *does not* constrain the interval values of V_{P0}, ϵ and δ if the VTI layers are homogeneous and separated by plane non-intersecting boundaries (see the first section). Here, however, the interfaces are allowed to be curved, while the layers are still assumed to be homogeneous.

Our goal is to determine whether or not the data

$$\mathbf{d}(\mathbf{Y},\, n) \equiv \{\tau_0(\mathbf{Y},\, n),\, \mathbf{p}(\mathbf{Y},\, n),\, \mathbf{W}(\mathbf{Y},\, n)\}\,, \tag{26}$$

acquired at a number of CMP locations $\mathbf{Y} = [Y_1, Y_2]$ can be inverted for all relevant interval parameters

$$\mathbf{m} \equiv \{V_{P0,n},\, \epsilon_n,\, \delta_n,\, \zeta_{j_1 j_2,\, n}\}\,, \tag{27}$$

$$(n = 1,\, \ldots,\, N;\;\; j_1 = 1,\, \ldots,\, J_1;\;\; j_2 = 1,\, \ldots,\, J_2)\,.$$

The matrices $\boldsymbol{\zeta}_n$ contain the coefficients of the basis functions describing the depths $z_n(Y_1, Y_2)$ of the model interfaces.

Since the quantities $\boldsymbol{\zeta}_n$ have to be estimated from the data, the inversion procedure can be simplified by adopting a linear relationship between $z_n(Y_1, Y_2)$ and $\zeta_{j_1 j_2, n}$. In principle, this requirement can be satisfied by representing the interfaces in terms of arbitrary basis functions $B_{j_1}(Y_1)$ and $B_{j_2}(Y_2)$:

$$z_n(Y_1, Y_2) = \sum_{j_1=1}^{J_1} \sum_{j_2=1}^{J_2} \zeta_{j_1 j_2,\, n}\, B_{j_1}(Y_1)\, B_{j_2}(Y_2)\,. \tag{28}$$

For simplicity, here we elected to implement the polynomial representation

$$z_n(Y_1, Y_2) = \sum_{j_1=1}^{J_1} \sum_{j_2=1}^{J_2} \zeta_{j_1 j_2,\, n}\, Y_1^{j_1 - 1}\, Y_2^{j_2 - 1}\,. \tag{29}$$

Feasibility of parameter estimation

For models with plane interfaces, the dependence of the data vector (26) on the CMP coordinate $\mathbf{Y}$ does not provide any new information about the model parameters. This is no longer the case in the presence of interface curvature because zero-offset reflection rays change direction with CMP location. Therefore, the spatial variation of the data may help to constrain the inversion and determine the depth scale of the model.

Similar to the approach outlined above for plane interfaces, the zero-offset traveltimes $\tau_0(n)$ and the reflection slopes $\mathbf{p}(n)$ can be used to find the shape of the interfaces $z_n(\mathbf{Y})$ for any given estimate of the layer parameters (i.e., a trial model)

$$\mathbf{l} = \{V_{P0,n},\, \epsilon_n,\, \delta_n\}\,, \quad (n = 1,\, \ldots,\, N)\,. \tag{30}$$

This is achieved by tracing zero-offset rays downward and computing the coordinates of the reflection points and the corresponding interface normals. In contrast to media with plane interfaces, however, the number of common midpoints and their spatial distribution determine our ability to reconstruct the shape of curved interfaces.

Since the slowness vector of each zero-offset ray is orthogonal to the reflector at the reflection point R (Fig. 10), it provides the orientation (i.e., the azimuth and polar angle) of the unit normal $\mathbf{b}_n(R)$ to the reflecting interface. In addition, the zero-offset traveltime yields the depth of the reflection point R. Therefore, the triplet $\{\tau_0(n, \mathbf{Y}),\, p_1(n, \mathbf{Y}),\, p_2(n, \mathbf{Y})\}$ at the CMP location $\mathbf{Y}$ provides three constraints on the quantities $\zeta_{j_1 j_2, n}$ specifying the reflector $z_n(\mathbf{Y})$ [equation (29)]. This implies that the number M of common midpoints required to obtain $J_1 \times J_2$ coefficients $\boldsymbol{\zeta}_n$ has to satisfy the inequality

$$M \geq \frac{J_1\, J_2}{3}\,. \tag{31}$$

For example, four appropriately chosen common midpoints ($M = 4$) in Fig. 11 should be sufficient for reconstructing $J_1\, J_2 = 3 \times 3 = 9$ coefficients that define each model interface. We solve the equations for the coefficients $\boldsymbol{\zeta}_n$ by least squares using all available CMP locations.

While the traveltimes $\tau_0(n, \mathbf{Y})$ and slopes $\mathbf{p}(n, \mathbf{Y})$ are used to obtain $z_n(\mathbf{Y})$, the information required to estimate the interval parameters $\mathbf{l}$ [equation (30)] is provided by the NMO ellipses $\mathbf{W}(n)$. To prove that the NMO ellipses may constrain the layer parameters uniquely, we present an example of singular value decomposition (SVD) analysis for the two-layer VTI model shown in Fig. 11. The ellipses measured from

the two reflectors at four CMP locations (triangles in Fig. 11) provide $2 \times 4 \times 3 = 24$ equations for the six components of the vector $\mathbf{l}$.

Thus, the feasibility of the inversion can be evaluated by applying SVD to the 24×6 matrix $\mathcal{F}$ of Frechét derivatives

$$\mathcal{F} = \frac{\partial \mathbf{W}(n, \mathbf{Y})}{\partial \mathbf{l}} \tag{32}$$

computed for correct values of model parameters $\mathbf{m}$. Since none of the singular values vanishes (Fig. 12), the input data provide sufficient information for parameter estimation, and this VTI model can be fully reconstructed in the depth domain from P-wave reflection traveltimes.

Clearly, it is not *always* possible to obtain VTI parameters using just P-wave data. For example, as the curvature of the intermediate interface in Fig. 11 decreases, our model approaches that with plane interfaces wherein at least one singular value is zero (see above). One of the singular values also vanishes when either layer is elliptically anisotropic, so that $\epsilon_n = \delta_n$ (Dellinger and Muir 1988).

Inversion examples

To confirm the SVD results, we carried out actual inversion of P-wave data for the model in Fig. 11 in the presence of noise. Reflection traveltimes were computed for 240 common midpoints placed at every 25 m along the two dashed lines between the triangles in Fig. 11. This provided an overdetermined system of $240 \times 3 = 720$ equations for reconstructing the matrix $\boldsymbol{\zeta}$ describing each interface. We added Gaussian noise to the modeled NMO velocities and zero-offset traveltimes, and obtained the parameter vector $\mathbf{m}$ [equation (27)] using the two-step inversion procedure discussed above.

Comparing the results of this test with the actual parameters (Table 4), we conclude that all three parameters in both layers were found with good accuracy. The

relative errors in the interval vertical velocities $V_{P0,n}$ and absolute errors in the anisotropic coefficients are comparable to the standard deviation of the noise added to the NMO velocities. The inversion results (for the same input data) do not depend on the initial guess for the model parameters, which suggests that the least-squares objective function in a certain vicinity of the correct solution is unimodal. Knowledge of the interval VTI parameters $V_{P0,n}$, ϵ_n and δ_n is sufficient to reconstruct the depth and shape of the interfaces and build the entire VTI model in depth.

Another example, this time for a three-layer VTI model with more complicated shape of the interfaces is shown in Fig. 13 and Table 5. The data vector $\mathbf{d}(\mathbf{Y}, n)$ was determined from the traveltimes computed at 600 common midpoints located along two lines with a spacing of 15 m. The accuracy of parameter estimation on noise-contaminated data (Table 5) is comparable to that in the example from Table 4. Therefore, for a subset of layered VTI models with curved interfaces, P-wave reflection traveltimes provide sufficient information for the inversion in the depth domain.

DISCUSSION AND CONCLUSIONS

The possibility of inverting P-wave reflection data for the interval parameters of layered VTI media strongly depends on the geometry of intermediate interfaces. While only the zero-dip NMO velocity $V_{\rm nmo}(0)$ and the anellipticity coefficient η can be obtained for laterally homogeneous VTI media above a dipping reflector, the presence of dipping or curved interfaces in the overburden may help to estimate all three relevant anisotropic parameters ($V_{0,n}$, ϵ_n and δ_n). Here, we examined the inversion of P-wave NMO ellipses and zero-offset traveltimes (measured from multi-azimuth 3-D reflection data) for the interval VTI parameters and the shape and depth of the interfaces. Since this method operates with NMO (stacking) velocities determined on moderate-length CMP spreads, it can be called "stacking-velocity tomography."

The objective function, which has to be minimized during the inversion, is ob-

tained in two steps. First, for each trial set of the interval VTI parameters P-wave zero-offset traveltimes and reflection slopes (horizontal slownesses) are used to reconstruct the reflectors and build the trial model in depth. Second, we compute the effective NMO ellipses of reflection events and define the objective function as a measure of the difference between the modeled ellipses and those estimated from the data.

Plane interfaces

If the interfaces are *plane*, have different azimuths, and do not cross each other, the P-wave NMO ellipses in an N-layer model yield $3N-1$ independent equations for the $3N$ interval parameters $V_{0,n}$, ϵ_n and δ_n. Unfortunately, the spatial variation of the NMO ellipses for this model does not provide any additional information for the inversion procedure. Therefore, in general, surface 3-D P-wave data alone are insufficient to determine the unknown VTI parameters and reconstruct the plane interfaces uniquely.

This ambiguity, however, can be overcome if a *single* parameter in any layer is known *a priori*. For example, in many cases the subsurface layer may be assumed to be isotropic ($\epsilon_1 = \delta_1 = 0$), or the vertical velocity in it may be estimated in a shallow borehole. The inversion can also be made unique by introducing some relationship between the parameters (e.g., between ϵ and δ) in at least one of the layers. The only model for which this approach fails to remove the ambiguity is elliptical anisotropy ($\epsilon_n = \delta_n$).

For 2-D models with co-oriented interfaces, the axes of all NMO ellipses are parallel to the dip and strike directions, and the number of independent equations reduces to $2N$. Therefore, for 2-D inversion it is necessary to specify one parameter for each layer beforehand; for instance, the vertical velocities may be known from VSP measurements. The inversion is generally better constrained if the medium contains

multiple dips (e.g., a throughgoing fault plane). For some types of models with intersecting interfaces the parameter estimation can be performed without any *a priori* information.

Curved interfaces

To compute azimuthally dependent NMO velocity in models with *curved* interfaces, we generalized the theory of NMO-velocity surfaces (Grechka and Tsvankin 1999b) by deriving a correction for the interface curvature. The new methodology is designed to compute NMO ellipses over arbitrary anisotropic media with curved interfaces by tracing a *single* zero-offset ray for each reflection event. This modeling algorithm, which is orders of magnitude faster than 3-D two-point ray tracing, provides a foundation for efficient traveltime inversion.

The feasibility of the interval parameter estimation was studied using singular value decomposition (SVD) followed by the inversion of noise-contaminated data. The input parameters for the inversion include azimuthally dependent P-wave NMO velocities (i.e., NMO ellipses) and zero-offset traveltimes acquired at a number of common midpoints over the study area. In contrast to media with plane interfaces, for a subset of VTI models with curved interfaces it is possible to reconstruct the model in depth without using additional information. Interface curvature increases the angle coverage of reflected rays, which helps to constrain the parameters of the anisotropic velocity field. Only if the anisotropy of one or more layers is close to elliptical, does the depth scale become poorly constrained by P-wave data regardless of the interface shape, which agrees with the results of Dellinger and Muir (1988).

The most critical assumption that ensured the success of the inversion procedure is that the model is composed of *homogeneous* layers. Allowing for a variation in the VTI parameters within some of the layers may prevent us from resolving the three principal components of the model: anisotropy, irregular (curved) interfaces

and lateral velocity variation. Even for isotropic models with irregular interfaces and laterally varying velocity, the traveltime inversion is generally non-unique (Goldin 1986). Still, in some special cases it may be possible to separate the contributions of each of those three factors to the reflection traveltimes; this topic requires further investigation.

On the whole, our results indicate that for a range of laterally heterogeneous VTI models it is possible to build velocity models in depth (and, therefore, perform anisotropic depth imaging) using surface P-wave data.

ACKNOWLEDGMENTS

We are grateful to members of the A(nisotropy)-Team at the Center for Wave Phenomena (CWP), Colorado School of Mines, for helpful discussions and to Ken Larner (CSM) for his review of the manuscript. We also thank Joe Dellinger (BP Amoco) for discussing with us his results on elliptical anisotropy. The support for this work was provided by the members of the Consortium Project on Seismic Inverse Methods for Complex Structures at CWP and by the Chemical Sciences, Geosciences and Biosciences Division, Office of Basic Energy Sciences, U.S. Department of Energy.

APPENDIX A–NMO VELOCITY ON A CURVED CMP LINE

Here we extend the derivation of the NMO velocity measured along a *straight* arbitrarily oriented CMP line given by Grechka and Tsvankin (1999b) to CMP lines with nonzero curvature at the common midpoint. Our derivation is based on expanding the pure-mode reflection traveltime t in a Taylor series in half offset h ($h = 0$ at the CMP location). The traveltime is assumed to be smooth enough for all needed derivatives to exist at zero offset.

Let us denote by $\boldsymbol{\sigma}(0)$ the coordinate of the common midpoint O (Fig. A-1) on the curved CMP line $\boldsymbol{\sigma}$. If the CMP line is parameterized as a function of its arclength h, the coordinates of the source S and receiver R become $\boldsymbol{\sigma}(-h)$ and $\boldsymbol{\sigma}(h)$. Since we are interested in the small-offset approximation of the reflection traveltime, the function $\boldsymbol{\sigma}(h)$ can be replaced by its quadratic Taylor series expansion in the vicinity of $h = 0$:

$$\boldsymbol{\sigma}(h) = \boldsymbol{\sigma}(0) + \mathcal{L}\, h + \frac{1}{2}\,\mathcal{K}\, h^2 + o(h^2)\,. \tag{A-1}$$

Here $\mathcal{L}$ is the unit vector tangent to the CMP line at $h = 0$,

$$\mathcal{L} \equiv \left.\frac{d\boldsymbol{\sigma}}{dh}\right|_{h=0}, \tag{A-2}$$

and $\mathcal{K}$ is related to the curvature of the CMP line,

$$\mathcal{K} \equiv \left.\frac{d^2\boldsymbol{\sigma}}{dh^2}\right|_{h=0}. \tag{A-3}$$

The pure-mode two-way reflection traveltime t measured at small offsets h along the CMP line $\boldsymbol{\sigma}$ can be expanded in a similar quadratic Taylor series,

$$t\Big(\boldsymbol{\sigma}(h), \mathbf{r}\Big) = t\Big(\boldsymbol{\sigma}(0), \mathbf{r}\Big) + \left.\frac{dt\Big(\boldsymbol{\sigma}(h), \mathbf{r}\Big)}{dh}\right|_{h=0} h + \frac{1}{2}\left.\frac{d^2t\Big(\boldsymbol{\sigma}(h), \mathbf{r}\Big)}{dh^2}\right|_{h=0} h^2 + \ldots \tag{A-4}$$

The traveltime t depends on the source and receiver positions and on the coordinate $\mathbf{r}$ of the reflection point. Summing up the one-way traveltimes τ corresponding to the down- and upgoing rays, we can write

$$t\Big(\boldsymbol{\sigma}(h),\mathbf{r}\Big)=\tau\Big(\boldsymbol{\sigma}(-h),\mathbf{r}\Big)+\tau\Big(\boldsymbol{\sigma}(h),\mathbf{r}\Big)\,. \tag{A-5}$$

We begin with showing (following the derivation of Tsvankin and Grechka 2000) that the reflection point dispersal (i.e., the deviation of $\mathbf{r}$ from the zero-offset reflection point $\mathbf{r}_0$ in Fig. A-1) has no influence on the values of the derivatives dt/dh and d^2t/dh^2 at $h=0$, so equation (A-5) can be replaced with

$$t\Big(\boldsymbol{\sigma}(h),\mathbf{r}\Big)=t\Big(\boldsymbol{\sigma}(h),\mathbf{r}_0\Big)=\tau\Big(\boldsymbol{\sigma}(-h),\mathbf{r}_0\Big)+\tau\Big(\boldsymbol{\sigma}(h),\mathbf{r}_0\Big)\,. \tag{A-6}$$

Let us examine the difference

$$\Delta t\equiv t\Big(\boldsymbol{\sigma}(h),\mathbf{r}\Big)-t\Big(\boldsymbol{\sigma}(h),\mathbf{r}_0\Big)\,\Big|_{\text{fixed }\boldsymbol{\sigma}\text{ and }h} \tag{A-7}$$

between the traveltimes corresponding to the specular reflection point $\mathbf{r}$ and to the zero-offset (non-specular) reflection point $\mathbf{r}_0$. The source and receiver are located along the CMP line $\boldsymbol{\sigma}$ at the fixed half-offset h. The difference Δt can be expanded in a Taylor series in the distance $\rho=|\mathbf{r}-\mathbf{r}_0|$ between the points $\mathbf{r}$ and $\mathbf{r}_0$ (Fig. A-1). At zero-offset, $\mathbf{r}=\mathbf{r}_0$ and $\Delta t|_{\rho=0}=0$ as follows from equation (A-7). Since the traveltime has an extremum at the specular reflection point $\mathbf{r}$ (Fermat's principle), the series $\Delta t(\rho)$ starts with the quadratic term

$$\Delta t(\rho)=\frac{1}{2}\,A\Big(\boldsymbol{\sigma}(h)\Big)\,\rho^2\Big(\boldsymbol{\sigma}(h)\Big)+o(\rho^2)\,, \tag{A-8}$$

where

$$A\Big(\boldsymbol{\sigma}(h)\Big)=-\frac{d^2t\Big(\boldsymbol{\sigma}(h),\mathbf{r}\Big)}{d\rho^2}\,\bigg|_{\mathbf{r}}\,. \tag{A-9}$$

Differentiating equation (A-8) with respect to h yields

$$\frac{d\Delta t}{dh}=\frac{dA\Big(\boldsymbol{\sigma}(h)\Big)}{dh}\,\rho^2\Big(\boldsymbol{\sigma}(h)\Big)+2\,A\Big(\boldsymbol{\sigma}(h)\Big)\,\rho\Big(\boldsymbol{\sigma}(h)\Big)\,\frac{d\rho\Big(\boldsymbol{\sigma}(h)\Big)}{dh}\,. \tag{A-10}$$

Since $\rho=0$ at $h=0$, the derivative

$$\frac{d\Delta t}{dh}\,\bigg|_{h=0}=0\,. \tag{A-11}$$

Therefore,

$$\left.\frac{dt\Big(\boldsymbol{\sigma}(h),\mathbf{r}\Big)}{dh}\right|_{h=0} = \left.\frac{dt\Big(\boldsymbol{\sigma}(h),\mathbf{r}_0\Big)}{dh}\right|_{h=0} . \tag{A-12}$$

Next, we differentiate equation (A-10) again:

$$\begin{aligned}\frac{d^2\Delta t}{dh^2} = {} & \frac{d^2A\Big(\boldsymbol{\sigma}(h)\Big)}{dh^2}\,\rho^2\Big(\boldsymbol{\sigma}(h)\Big) + 4\,\frac{dA\Big(\boldsymbol{\sigma}(h)\Big)}{dh}\,\rho\Big(\boldsymbol{\sigma}(h)\Big)\,\frac{d\rho\Big(\boldsymbol{\sigma}(h)\Big)}{dh} \\ & +2\,A\Big(\boldsymbol{\sigma}(h)\Big)\,\left[\frac{d\rho\Big(\boldsymbol{\sigma}(h)\Big)}{dh}\right]^2 + 2\,A\Big(\boldsymbol{\sigma}(h)\Big)\,\rho\Big(\boldsymbol{\sigma}(h)\Big)\,\frac{d^2\rho\Big(\boldsymbol{\sigma}(h)\Big)}{dh^2} .\end{aligned} \tag{A-13}$$

Evaluating the derivative (A-13) at $h = \rho = 0$, we obtain

$$\left.\frac{d^2\Delta t}{dh^2}\right|_{h=0} = 2\,A\Big(\boldsymbol{\sigma}(h)\Big)\left[\frac{d\rho\Big(\boldsymbol{\sigma}(h)\Big)}{dh}\right]^2\Bigg|_{h=0} . \tag{A-14}$$

To show that the derivative (A-14) is zero, we note that both the traveltime and the ray trajectory of a pure reflection mode remain the same if we interchange the source and receiver positions (the reciprocity principle). Hence,

$$\mathbf{r}\Big(\boldsymbol{\sigma}(h)\Big) = \mathbf{r}\Big(\boldsymbol{\sigma}(-h)\Big) \tag{A-15}$$

and, therefore,

$$\rho\Big(\boldsymbol{\sigma}(h)\Big) \equiv \Big|\mathbf{r}\Big(\boldsymbol{\sigma}(h)\Big) - \mathbf{r}_0\Big| = \Big|\mathbf{r}\Big(\boldsymbol{\sigma}(-h)\Big) - \mathbf{r}_0\Big| = \rho\Big(\boldsymbol{\sigma}(-h)\Big) , \tag{A-16}$$

i.e., ρ is an even function of h for any fixed CMP line $\boldsymbol{\sigma}$. Consequently,

$$\left.\frac{d\rho\Big(\boldsymbol{\sigma}(h)\Big)}{dh}\right|_{h=0} = 0 , \tag{A-17}$$

so equation (A-14) results in

$$\left.\frac{d^2\Delta t}{dh^2}\right|_{h=0} = 0 . \tag{A-18}$$

Thus, we have proven that

$$\left.\frac{d^2t\Big(\boldsymbol{\sigma}(h),\mathbf{r}\Big)}{dh^2}\right|_{h=0} = \left.\frac{d^2t\Big(\boldsymbol{\sigma}(h),\mathbf{r}_0\Big)}{dh^2}\right|_{h=0} , \tag{A-19}$$

and the derivatives in the series (A-4) can be obtained by differentiating equation (A-6). This result is equivalent to the normal-incidence-point (NIP) theorem proved by Chernyak and Gritsenko (1979) [their proof can be also found in Goldin (1986)] and by Hubral and Krey (1980).

The zero-offset ($h = 0$) traveltime can be expressed as [see equation (A-6)]

$$t\Big(\boldsymbol{\sigma}(h), \mathbf{r}_0\Big)\Big|_{h=0} \equiv t_0 = 2\,\tau(\boldsymbol{\sigma}(0)). \tag{A-20}$$

Differentiating equation (A-6) and taking into account equation (A-1), we find

$$\frac{dt\Big(\boldsymbol{\sigma}(h)\Big)}{dh}\bigg|_{h=0} = \sum_{k=1}^{3} \frac{\partial \tau}{\partial \sigma_k} \Big(-\mathcal{L}_k + \mathcal{L}_k + 2\,\mathcal{K}_k\,h + o(h)\Big)\bigg|_{h=0} = 0\,. \tag{A-21}$$

Differentiating the one-way traveltime with respect to h twice yields

$$\frac{d^2\tau\Big(\boldsymbol{\sigma}(h)\Big)}{dh^2} = \sum_{k,m=1}^{3} \frac{\partial^2\tau\Big(\boldsymbol{\sigma}(h)\Big)}{\partial\sigma_k\,\partial\sigma_m} \frac{d\sigma_k}{dh} \frac{d\sigma_m}{dh} + \sum_{k=1}^{3} \frac{\partial\tau\Big(\boldsymbol{\sigma}(h)\Big)}{\partial\sigma_k} \frac{d^2\sigma_k}{dh^2}\,. \tag{A-22}$$

Using equations (A-1), (A-6) and (A-22) leads to

$$\frac{d^2t\Big(\boldsymbol{\sigma}(h)\Big)}{dh^2}\bigg|_{h=0} = 2 \sum_{k,m=1}^{3} \frac{\partial^2\tau\Big(\boldsymbol{\sigma}(h)\Big)}{\partial\sigma_k\,\partial\sigma_m}\bigg|_{h=0} \mathcal{L}_k\,\mathcal{L}_m + 2 \sum_{k=1}^{3} \frac{\partial\tau\Big(\boldsymbol{\sigma}(h)\Big)}{\partial\sigma_k}\bigg|_{h=0} \mathcal{K}_k\,. \tag{A-23}$$

Noting that

$$\frac{\partial}{\partial\sigma_k}\bigg|_{h=0} = \frac{\partial}{\partial x_k}\bigg|_{h=0} \tag{A-24}$$

equation (A-23) can be rewritten in the following form:

$$\frac{d^2t\Big(\boldsymbol{\sigma}(h)\Big)}{dh^2}\bigg|_{h=0} = 2 \sum_{k,m=1}^{3} \frac{\partial^2\tau(\mathbf{x})}{\partial x_k\,\partial x_m}\bigg|_{h=0} \mathcal{L}_k\,\mathcal{L}_m + 2 \sum_{k=1}^{3} \frac{\partial\tau(\mathbf{x})}{\partial x_k}\bigg|_{h=0} \mathcal{K}_k\,. \tag{A-25}$$

Equation (A-25) relates the second-order derivative of the two-way traveltime t with respect to the half-offset and the second-order spatial derivatives of the one-way traveltime τ from the zero-offset reflection point.

To obtain an equation for the NMO velocity along the CMP line $\boldsymbol{\sigma}$, we substitute the derivatives (A-21) and (A-25) into the series (A-4):

$$t\Big(\boldsymbol{\sigma}(h)\Big) = t_0 + h^2 \left\{ \sum_{k,m=1}^{3} \left. \frac{\partial^2 \tau(\mathbf{x})}{\partial x_k \, \partial x_m} \right|_{h=0} \mathcal{L}_k \, \mathcal{L}_m + \sum_{k=1}^{3} \left. \frac{\partial \tau(\mathbf{x})}{\partial x_k} \right|_{h=0} \mathcal{K}_k \right\} . \qquad \text{(A-26)}$$

Squaring this equation and keeping the quadratic and lower-order terms with respect to h yields

$$t^2\Big(\boldsymbol{\sigma}(h)\Big) = t_0^2 + 2\, t_0\, h^2 \left\{ \sum_{k,m=1}^{3} \left. \frac{\partial^2 \tau(\mathbf{x})}{\partial x_k \, \partial x_m} \right|_{h=0} \mathcal{L}_k \, \mathcal{L}_m + \sum_{k=1}^{3} \left. \frac{\partial \tau(\mathbf{x})}{\partial x_k} \right|_{h=0} \mathcal{K}_k \right\} . \qquad \text{(A-27)}$$

Introducing the source-receiver offset

$$X = 2\, h\,, \qquad \text{(A-28)}$$

we rewrite equation (A-27) in its final form,

$$t^2\Big(\boldsymbol{\sigma}(X)\Big) = t_0^2 + (\mathcal{L}\, \mathbf{U}\, \mathcal{L}^{\mathbf{T}} + \tau_0\, \mathbf{p} \cdot \mathcal{K})\, X^2\,, \qquad \text{(A-29)}$$

where $\tau_0 = t_0/2$ is the one-way zero-offset traveltime. Here $\mathbf{T}$ denotes transposition, and the 3×3 symmetric matrix $\mathbf{U}$ is defined as

$$U_{km} \equiv \tau_0 \left. \frac{\partial^2 \tau(\mathbf{x})}{\partial x_k \, \partial x_m} \right|_{h=0} = \tau_0 \left. \frac{\partial p_k(\mathbf{x})}{\partial x_m} \right|_{h=0} , \qquad (k, m = 1, 2, 3)\,; \qquad \text{(A-30)}$$

$$p_k(\mathbf{x}) \equiv \frac{\partial \tau(\mathbf{x})}{\partial x_k}\,, \qquad (k, m = 1, 2, 3), \qquad \text{(A-31)}$$

are the components of the slowness vector $\mathbf{p} = [p_1, p_2, p_3]$. In equation (A-29) $\mathbf{p}$ is evaluated at the CMP location.

Comparing equation (A-29) with the conventional definition of the NMO velocity $V_{\rm nmo}(\boldsymbol{\sigma})$ along the CMP line $\boldsymbol{\sigma}$,

$$t^2\Big(\boldsymbol{\sigma}(X)\Big) = t_0^2 + \frac{X^2}{V_{\rm nmo}^2(\boldsymbol{\sigma})}\,, \qquad \text{(A-32)}$$

we conclude that

$$V_{\rm nmo}^{-2}(\boldsymbol{\sigma}) = \mathcal{L}\, \mathbf{U}\, \mathcal{L}^{\mathbf{T}} + \tau_0\, \mathbf{p} \cdot \mathcal{K}\,. \qquad \text{(A-33)}$$

APPENDIX B–NMO VELOCITY AT A CURVED SURFACE

Equation (A-33) can be used to describe the azimuthal variation of the NMO velocity measured along CMP lines at a curved surface $\mathbf{s}$. Let us specify the surface

$$\mathbf{s} \equiv \mathbf{s}(h_1, h_2) \tag{B-1}$$

by a pair of curvilinear orthogonal coordinates h_1 and h_2 (Fig. B-1) in such a way that the half-offset h along the CMP line $\boldsymbol{\sigma}$ is given as (for $h \to 0$)

$$h_1 = h \, \cos\alpha \tag{B-2}$$

and

$$h_2 = h \, \sin\alpha \,, \tag{B-3}$$

where α is the azimuth of the tangent to the CMP line at the common midpoint O with respect to the axis h_1 (Fig. B-1).

For simplicity, the axis x_3 of the coordinate frame is directed along the normal $\mathbf{b}$ to the surface $\mathbf{s}(h_1, h_2)$ at the CMP location. This implies that the tangent vector $\mathcal{L}$ to the CMP line at O [see equation (A-2)] is

$$\mathcal{L} = [\cos\alpha, \, \sin\alpha, \, 0] \,, \tag{B-4}$$

and we can replace $\mathcal{L}$ with the vector ℓ which lies in $\mathbf{s}$:

$$\ell \equiv [\mathcal{L}_1, \, \mathcal{L}_2] = [\cos\alpha, \, \sin\alpha] \,. \tag{B-5}$$

To obtain the NMO velocity for any CMP line $\boldsymbol{\sigma}$ within $\mathbf{s}$, we need to express the curvature $\mathcal{K}$ in equation (A-33) in terms of the derivatives of $\mathbf{s}$ with respect to the coordinates h_1 and h_2. Using equations (A-3), (B-2) and (B-3), we find

$$\begin{aligned} \mathcal{K} = \left. \frac{d^2\mathbf{s}}{dh^2} \right|_{\text{along } \boldsymbol{\sigma}, \; h=0} &= \left. \sum_{i,j=1}^{2} \frac{\partial^2 \mathbf{s}}{\partial h_i \, \partial h_j} \frac{dh_i}{dh} \frac{dh_j}{dh} \right|_{h=0} \\ &= \boldsymbol{\kappa}_{11} \, \cos^2\alpha + 2 \, \boldsymbol{\kappa}_{12} \, \sin\alpha \, \cos\alpha + \boldsymbol{\kappa}_{22} \, \sin^2\alpha \,, \end{aligned} \tag{B-6}$$

where

$$\boldsymbol{\kappa}_{ij} \equiv \left. \frac{\partial^2 \mathbf{s}}{\partial h_i \, \partial h_j} \right|_{h_1 = h_2 = 0} , \qquad (i, j = 1, 2) . \tag{B-7}$$

Equation (B-6) can be rewritten in matrix form using equation (B-5):

$$\mathcal{K} = \ell \, \boldsymbol{\kappa} \, \ell^{\mathbf{T}} . \tag{B-8}$$

Equation (A-33) then yields

$$V_{\mathrm{nmo}}^{-2}(\mathbf{s}, \ell) = \ell \, \left(\mathbf{W} + \tau_0 \, \mathbf{p} \cdot \boldsymbol{\kappa} \right) \, \ell^{\mathbf{T}} , \tag{B-9}$$

where

$$W_{ij} \equiv U_{ij} , \qquad (i, j = 1, 2) . \tag{B-10}$$

Thus, the directional dependence of the NMO velocity $V_{\mathrm{nmo}}(\mathbf{s}, \ell)$ measured on the curved surface $\mathbf{s}$ can be described in terms of the following 2×2 symmetric quadratic form:

$$\mathcal{W} \equiv \mathbf{W} + \tau_0 \, \mathbf{p} \cdot \boldsymbol{\kappa} , \tag{B-11}$$

where $\mathbf{W}$ is the matrix that represents the NMO ellipse in the plane tangent to $\mathbf{s}$ at the CMP location, and $\tau_0 \, \mathbf{p} \cdot \boldsymbol{\kappa}$ is the correction for the curvature.

APPENDIX C–CONTINUATION OF NMO VELOCITIES THROUGH CURVED INTERFACES

Grechka and Tsvankin (1999b) developed concise Dix-type formulae for anisotropic models composed of homogeneous layers separated by planar interfaces. They showed that the effective NMO ellipse at a given CMP location can be obtained by averaging the intersections of the NMO-velocity surfaces with the layer boundaries along the zero-offset ray. Here, we use the results of Appendices A and B to extend their procedure to media with curved interfaces.

The derivation of Grechka and Tsvankin (1999b) was based on the fact that the intersections of the NMO-velocity surfaces $\mathbf{U}$ with the planar boundaries (i.e., the NMO ellipses $\mathbf{W}$) are the same on both sides of each interface. For curved interfaces, the quantities continuous across the interfaces are the matrices $\mathcal{W}$ defined by equation (B-11). Indeed, $\mathcal{W}$ determine the NMO velocities measured on the top (+) and bottom (−) sides of the interface $\mathbf{s}$ (Fig. C-1). According to equation (B-11),

$$\mathcal{W}^{(+)} = \mathbf{W}^{(+)} + \tau_0 \, \mathbf{p}^{(+)} \cdot \boldsymbol{\kappa} \, , \tag{C-1}$$

$$\mathcal{W}^{(-)} = \mathbf{W}^{(-)} + \tau_0 \, \mathbf{p}^{(-)} \cdot \boldsymbol{\kappa} \, . \tag{C-2}$$

As shown in Appendix A, NMO velocity can be computed using the one-way traveltimes from the zero-offset reflection point to the CMP line. Essentially, those traveltimes correspond to the wavefront propagating from the zero-offset reflection point. To satisfy the boundary conditions, the wavefront has to be continuous across surface $\mathbf{s}$, which implies that the NMO velocities measured on two sides of $\mathbf{s}$ at the reflection/transmission point (Fig. C-1) are identical. Therefore,

$$\mathcal{W}^{(+)} = \mathcal{W}^{(-)} \, . \tag{C-3}$$

In contrast, the NMO ellipses $\mathbf{W}^{(+)}$ and $\mathbf{W}^{(-)}$ measured on two sides of the plane $\mathcal{P}$ tangent to $\mathbf{s}$ have to be different because the slowness vector changes across the interface. Combining equations (C-1)–(C-3), we find

$$\mathbf{W}^{(+)} = \mathbf{W}^{(-)} - \tau_0 \left(\mathbf{p}^{(+)} - \mathbf{p}^{(-)} \right) \cdot \boldsymbol{\kappa} \,. \tag{C-4}$$

As discussed in the main text, the correction of NMO ellipses for the interface curvature developed here can be used to extend the Dix-type averaging formulae of Grechka, Tsvankin and Cohen (1999) and Grechka and Tsvankin (1999b) to media with curved interfaces.

REFERENCES

Alkhalifah T., Biondi B. and Fomel S. 1998. Time-domain processing in arbitrary inhomogeneous media. 68th SEG meeting, New Orleans, USA, Expanded Abstracts, 1756–1759.

Alkhalifah T. and Tsvankin I. 1995. Velocity analysis in transversely isotropic media. *Geophysics* **60**, 1550–1566.

Bartel D.C., Abriel W.L., Meadows M.A. and Hill N.R. 1998. Determination of transversely isotropic velocity parameters at the Pluto Discovery, Gulf of Mexico. 68th SEG meeting, New Orleans, USA, Expanded Abstracts, 1269–1272.

Bube K.P. and Meadows M.A. 1997. On the null space in linearized anisotropic surface reflection tomography. 67th SEG meeting, Dallas, USA, Expanded Abstracts, 1677–1680.

Chernyak V.S. and Gritsenko S.A. 1979. Interpretation of effective parameters of the CDP-method for system of 3-D homogeneous layers separated by irregular interfaces. *Geology and Geophysics* **12**, 112–120 (in Russian).

Dellinger J. and Muir F. 1988. Imaging reflections in elliptically anisotropic media. *Geophysics* **53**, 1616–1618.

Goldin S.V. 1986. *Seismic Traveltime Inversion.* Society of Exploration Geophysics.

Gray S.H., Maclean G. and Marfurt K.J. 1999. Crooked line, rough topography: advancing towards the correct seismic image. *Geophysical Prospecting* **47**, 721–733.

Grechka V. and Tsvankin I. 1998. 3-D description of normal moveout in anisotropic inhomogeneous media. *Geophysics* **63**, 1079-1092.

Grechka V. and Tsvankin I. 1999a. 3-D moveout inversion in azimuthally anisotropic media with lateral velocity variation: Theory and a case study. *Geophysics* **64**, 1202–1218.

Grechka V. and Tsvankin I. 1999b. NMO surfaces and Dix-type formulae in heterogeneous anisotropic media. 69th SEG meeting, Houston, USA, Expanded Abstracts, 1612–1615.

Grechka V., Tsvankin I. and Cohen J.K. 1999. Generalized Dix equation and analytic treatment of normal-moveout velocity for anisotropic media. *Geophysical Prospecting* **47**, 117–148.

Hubral P. and Krey T. 1980. *Interval velocities from seismic reflection measurements*. Society of Exploration Geophysicists.

Le Stunff Y., Grechka V. and Tsvankin I. 2001. Depth-domain velocity analysis in VTI media using surface P-wave data: Is it feasible? *Geophysics*, in print.

Le Stunff Y. and Grenié D. 1998. Taking into account a priori information in 3D tomography. 68th SEG meeting, New Orleans, USA, Expanded Abstracts, 1875–1878.

Le Stunff Y. and Jeannot J.P. 1998. Pre-stack anisotropic depth imaging. 60th EAGE Conference, Leipzig, Germany, Extended Abstracts.

Ryan-Grigor S. 1998. Empirical relationships between anellipticity and V_P/V_S in shales: Potential applications to AVO studies and anisotropic seismic processing. 68th SEG meeting, New Orleans, USA, Expanded Abstracts, 208–211.

Sexton P. and Williamson P. 1998. 3D anisotropic velocity estimation by model-based inversion of pre-stack traveltimes. 68th SEG meeting, New Orleans, USA, Expanded Abstracts, 1855–1858.

Thomsen L. 1986. Weak elastic anisotropy. *Geophysics* **51**, 1954–1966.

Tsvankin I. 2001. *Seismic signatures and analysis of reflection data in anisotropic media*. Elsevier Science.

Tsvankin I. and Grechka V. 2000. Dip moveout of converted waves and parameter estimation in transversely isotropic media. *Geophysical Prospecting* **48**, 257–292.

	$V_{P0,1}$ (km/s)	ϵ_1	δ_1	$V_{P0,2}$ (km/s)	ϵ_2	δ_2	$V_{P0,3}$ (km/s)	ϵ_3	δ_3
Correct	1.00	0.08	0.04	2.00	0.20	0.10	3.00	0.10	0.05
Inverted	0.99	0.09	–	2.02	0.18	0.09	2.96	0.18	0.07

	z_1 (km)	ϕ_1 (deg)	ψ_1 (deg)	z_2 (km)	ϕ_2 (deg)	ψ_2 (deg)	z_3 (km)	ϕ_3 (deg)	ψ_3 (deg)
Correct	1.00	30.0	–10.0	2.00	30.0	30.0	4.00	10.0	70.0
Inverted	1.00	29.8	–10.0	1.98	29.9	30.4	3.98	10.3	70.5

Table 1. Comparison of the correct and inverted parameters of a three-layer VTI model (see Fig. 5). The standard deviations of Gaussian noise added to the NMO velocities and zero-offset traveltimes are 2.0% and 0.5%, respectively.

	$V_{P0,1}$ (km/s)	ϵ_1	δ_1	$V_{P0,2}$ (km/s)	ϵ_2	δ_2	$V_{P0,3}$ (km/s)	ϵ_3	δ_3
Correct	1.00	0.08	0.04	2.00	0.20	0.10	3.00	0.10	0.05
Inverted	–	0.08	0.04	–	0.19	0.10	–	0.08	0.05

Table 2. Comparison of the correct and inverted values of parameters for the three-layer VTI model shown in Fig. 6. The standard deviations of Gaussian noise added to the NMO velocities and zero-offset traveltimes are 2.0% and 1.0%, respectively.

	$V_{P0,1}$ (km/s)	ϵ_1	$V_{P0,2}$ (km/s)	ϵ_2
Correct	1.00	0.20	2.00	0.20
Inverted	0.98	0.18	1.98	0.17

Table 3. Comparison of the correct and inverted values of parameters for the two-layer VTI model from Fig. 7. k_1 and k_2 are such that $\eta_1 = \eta_2 = 0.05$. NMO velocities, computed at 200 CMP locations, were contaminated by Gaussian noise with a standard deviation of 2%.

	$V_{P0,1}$ (km/s)	ϵ_1	δ_1	$V_{P0,2}$ (km/s)	ϵ_2	δ_2
Correct	1.00	0.20	0.10	2.00	0.15	0.05
Inverted	1.02	0.17	0.07	2.05	0.11	0.03

Table 4. Inversion results for the two-layer VTI model in Fig. 11. The standard deviations of Gaussian noise added to the NMO velocities and zero-offset traveltimes are 2.0% and 1.0%, respectively.

	$V_{P0,1}$ (km/s)	ϵ_1	δ_1	$V_{P0,2}$ (km/s)	ϵ_2	δ_2	$V_{P0,3}$ (km/s)	ϵ_3	δ_3
Correct	1.80	0.20	0.10	2.00	0.15	0.05	2.30	0.10	0.03
Inverted	1.77	0.23	0.12	1.97	0.17	0.07	2.26	0.12	0.05

Table 5. Inversion results for the three-layer VTI model in Fig. 13. The errors in the inverted quantities are due to Gaussian noise added to the NMO velocities (the standard deviation is 2.0%) and zero-offset traveltimes (the standard deviation is 1.0%)

FIGURES

FIG. 1. Zero-offset rays in a model containing a stack of VTI layers separated by plane dipping interfaces.

FIG. 2. Generalized Dix-type formula averages the intersections of the interval NMO-velocity cylinders with the model interfaces along the zero-offset raypath.

FIG. 3. SVD analysis for a two-layer VTI model with the parameters $V_{P0,1} = 2$ km/s, $\epsilon_1 = 0.15$, $\delta_1 = 0.05$, $V_{P0,2} = 3$ km/s, $\epsilon_2 = 0.25$, $\delta_2 = 0.10$. The singular values are normalized by the greatest one. The interface depths under the CMP location $\mathbf{O} = [0, 0, 0]$ are $z_1 = 1$ km and $z_2 = 3$ km, the dips $\phi_1 = 40^\circ$ and $\phi_2 = 20^\circ$, and the azimuth of the bottom interface is $\psi_2 = 0^\circ$. The curves correspond to different azimuths of the intermediate (first) interface: $\circ$ ($\psi_1 = 0^\circ$), $\square$ ($\psi_1 = 30^\circ$), $\diamond$ ($\psi_1 = 60^\circ$) and $\triangle$ ($\psi_1 = 90^\circ$).

FIG. 4. Contours of the fifth eigenvalue (multiplied by 1000) as a function of the dip ϕ_1 and azimuth ψ_1 of the intermediate interface in a two-layer VTI model. The parameters $V_{P0,1}$, ϵ_1, δ_1, $V_{P0,2}$, ϵ_2, δ_2, z_1, z_2, ϕ_2, and ψ_2 are the same as those in Fig. 3.

FIG. 5. Zero-offset P-wave rays in the three-layer VTI model with the parameters given in Table 1.

FIG. 6. Zero-offset rays in a three-layer VTI model. All interfaces have the same azimuth $\psi_1 = \psi_2 = \psi_3 = 0^\circ$.

FIG. 7. Contours of the smallest singular value (multiplied by 1000) for a two-layer VTI model. The relevant model parameters are $V_{P0,1} = 1$ km/s, $\epsilon_1 = 0.20$, $\delta_1 = k_1\,\epsilon_1$, $V_{P0,2} = 2$ km/s, $\epsilon_2 = 0.20$, $\delta_2 = k_2\,\epsilon_2$, $\phi_1 = 30^\circ$, $\psi_1 = 30^\circ$, $\phi_2 = 50^\circ$, $\psi_2 = 0^\circ$,

$z_1 = 1$ km, $z_2 = 3$ km. The coefficients k_1 and k_2 vary from 0 to 1.1.

FIG. 8. SVD analysis for a two-layer VTI model similar to the one in Fig. 3. This time, however, the intermediate interface contains two segments with the same dip $\phi_1 = 40^\circ$ but different azimuths $\psi_1 = 30^\circ$ and $\psi_1 = 90^\circ$.

FIG. 9. The presence of fault-plane reflections in layered VTI medium might be sufficient to reconstruct the model in depth using P-wave reflection data.

FIG. 10. Multi-azimuth CMP recording over a layered VTI model with curved interfaces.

FIG. 11. Zero-offset rays in the two-layer VTI model used in the SVD analysis (Fig. 12). CMP locations are marked by triangles. The relevant interval parameters are $V_{P0,1} = 1$ km/s, $\epsilon_1 = 0.20$, $\delta_1 = 0.10$, $V_{P0,2} = 2$ km/s, $\epsilon_2 = 0.15$, $\delta_2 = 0.05$. The interfaces are described by 2-D quadratic polynomials, so $\boldsymbol{\zeta}_1$ and $\boldsymbol{\zeta}_2$ are 3×3 matrices.

FIG. 12. Normalized singular values for the model from Fig. 11.

FIG. 13. Three-layer VTI model used in the inversion with several traced zero-offset rays. Common midpoints are located on the two gray dashed lines.

FIG. A-1. Reflection traveltimes are recorded along the curved CMP line $\boldsymbol{\sigma}$ with the common midpoint at O. Note the difference between the reflection points $\mathbf{r}_0$ and $\mathbf{r}$ of the zero-offset and nonzero-offset rays.

FIG. B-1. CMP line $\boldsymbol{\sigma}$ at an curved surface described by the radius-vector $\mathbf{s}(h_1, h_2)$.

$\mathbf{b}$ is the unit vector orthogonal to the surface at the common midpoint O.

FIG. C-1. Zero-offset ray crossing a curved interface $\mathbf{s}$. Plane $\mathcal{P}$ is tangent to the interface at the intersection point; $\mathbf{p}^{(+)}$ and $\mathbf{p}^{(-)}$ are the slowness vectors on different sides of the interface.

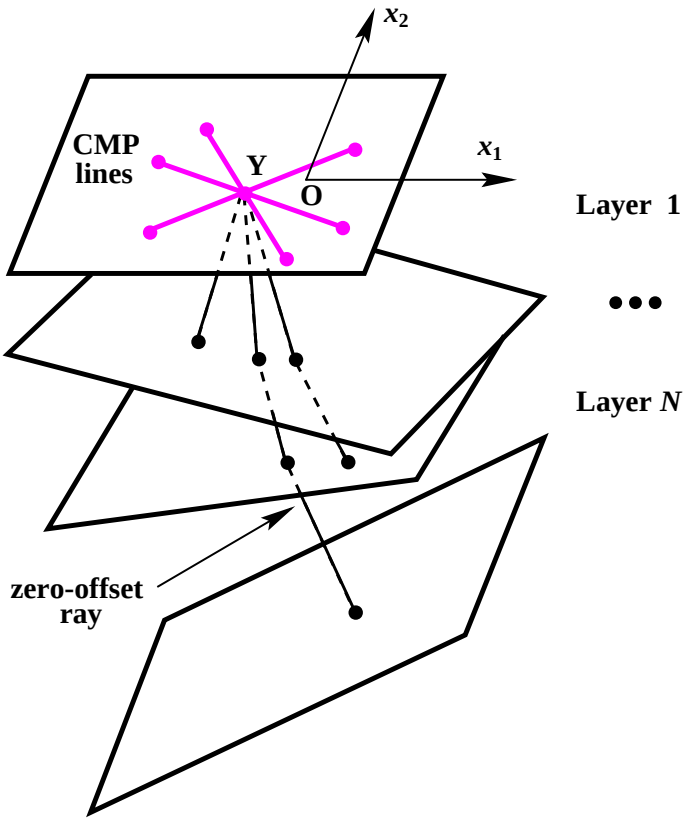

FIG. 1. Zero-offset rays in a model containing a stack of VTI layers separated by plane dipping interfaces.

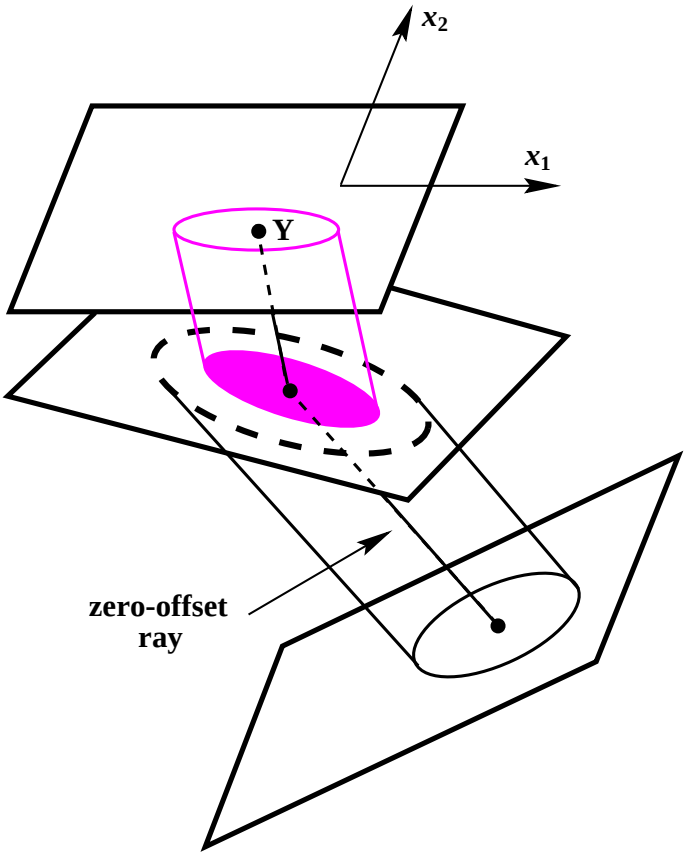

FIG. 2. Generalized Dix-type formula averages the intersections of the interval NMO-velocity cylinders with the model interfaces along the zero-offset raypath.

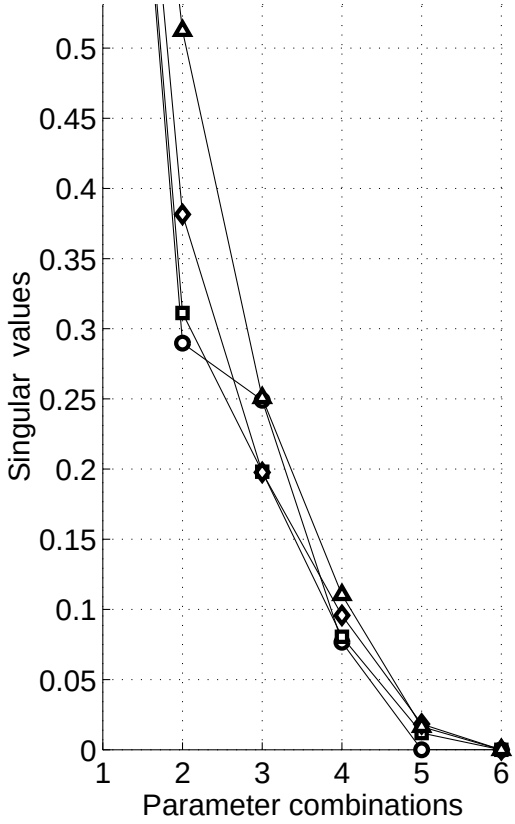

FIG. 3. SVD analysis for a two-layer VTI model with the parameters $V_{P0,1} = 2$ km/s, $\epsilon_1 = 0.15$, $\delta_1 = 0.05$, $V_{P0,2} = 3$ km/s, $\epsilon_2 = 0.25$, $\delta_2 = 0.10$. The singular values are normalized by the greatest one. The interface depths under the CMP location $\mathbf{O} = [0, 0, 0]$ are $z_1 = 1$ km and $z_2 = 3$ km, the dips $\phi_1 = 40°$ and $\phi_2 = 20°$, and the azimuth of the bottom interface is $\psi_2 = 0°$. The curves correspond to different azimuths of the intermediate (first) interface: $\circ$ ($\psi_1 = 0°$), $\square$ ($\psi_1 = 30°$), $\diamond$ ($\psi_1 = 60°$) and $\triangle$ ($\psi_1 = 90°$).

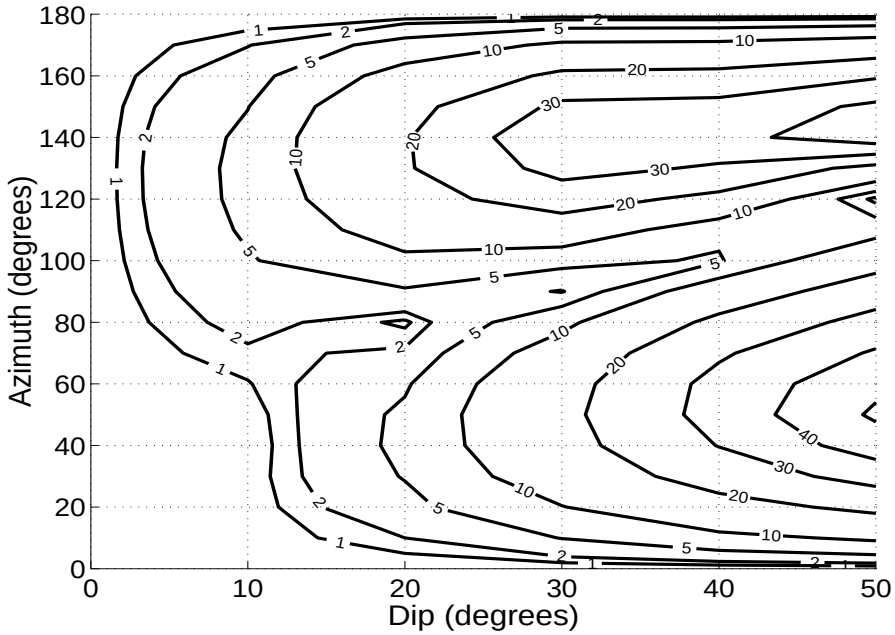

FIG. 4. Contours of the fifth eigenvalue (multiplied by 1000) as a function of the dip ϕ_1 and azimuth ψ_1 of the intermediate interface in a two-layer VTI model. The parameters $V_{P0,1}$, ϵ_1, δ_1, $V_{P0,2}$, ϵ_2, δ_2, z_1, z_2, ϕ_2, and ψ_2 are the same as those in Fig. 3.

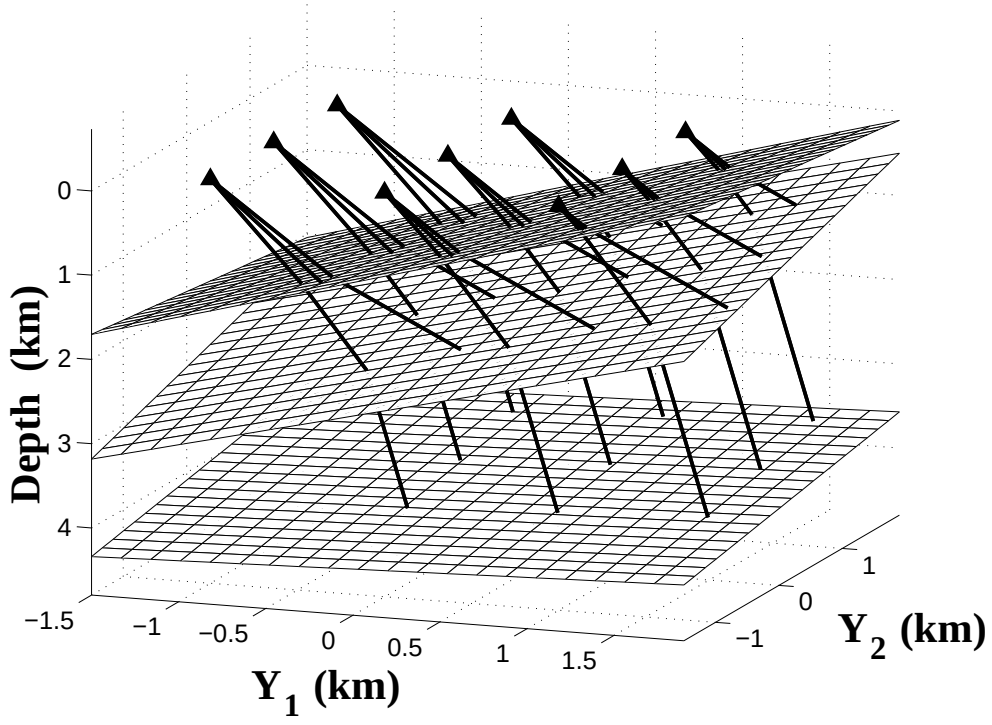

FIG. 5. Zero-offset P-wave rays in the three-layer VTI model with the parameters given in Table 1.

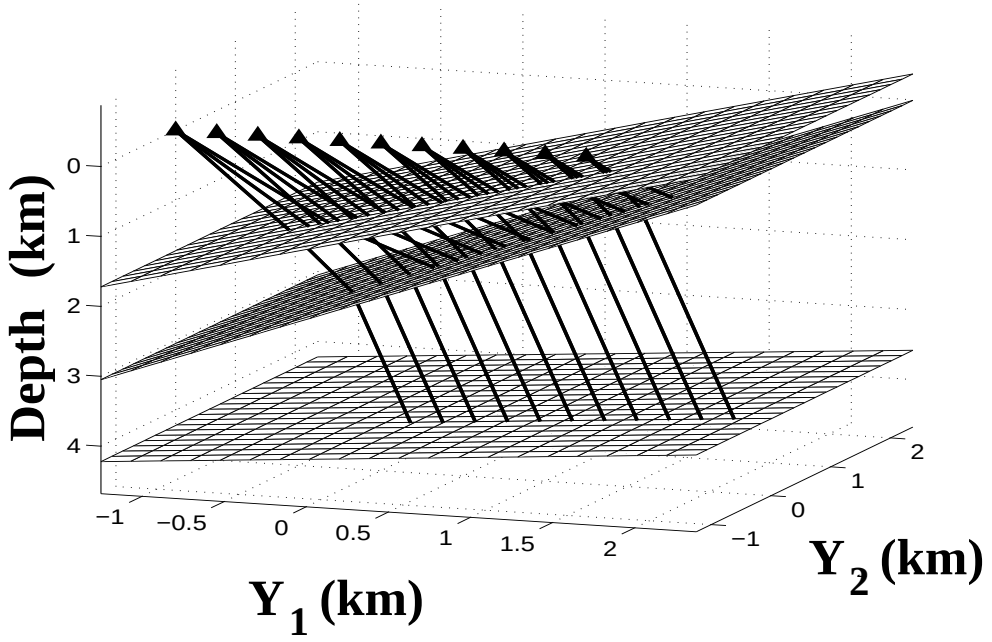

FIG. 6. Zero-offset rays in a three-layer VTI model. All interfaces have the same azimuth $\psi_1 = \psi_2 = \psi_3 = 0^\circ$.

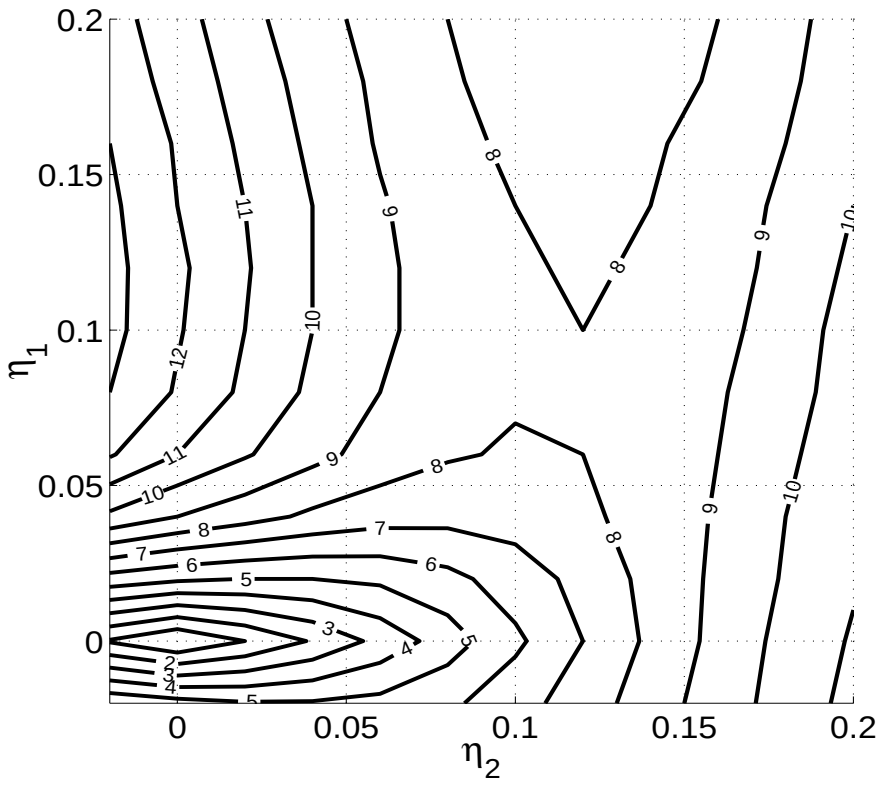

FIG. 7. Contours of the smallest singular value (multiplied by 1000) for a two-layer VTI model. The relevant model parameters are $V_{P0,1} = 1$ km/s, $\epsilon_1 = 0.20$, $\delta_1 = k_1\,\epsilon_1$, $V_{P0,2} = 2$ km/s, $\epsilon_2 = 0.20$, $\delta_2 = k_2\,\epsilon_2$, $\phi_1 = 30°$, $\psi_1 = 30°$, $\phi_2 = 50°$, $\psi_2 = 0°$, $z_1 = 1$ km, $z_2 = 3$ km. The coefficients k_1 and k_2 vary from 0 to 1.1.

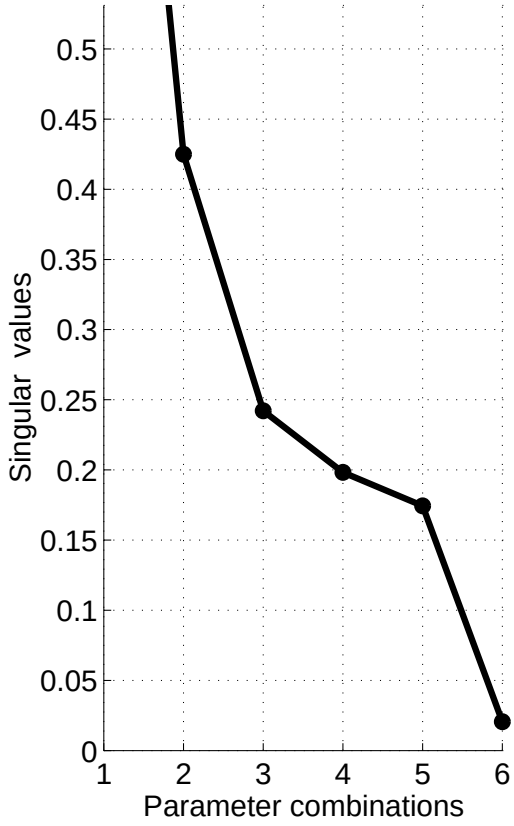

FIG. 8. SVD analysis for a two-layer VTI model similar to the one in Fig. 3. This time, however, the intermediate interface contains two segments with the same dip $\phi_1 = 40^\circ$ but different azimuths $\psi_1 = 30^\circ$ and $\psi_1 = 90^\circ$.

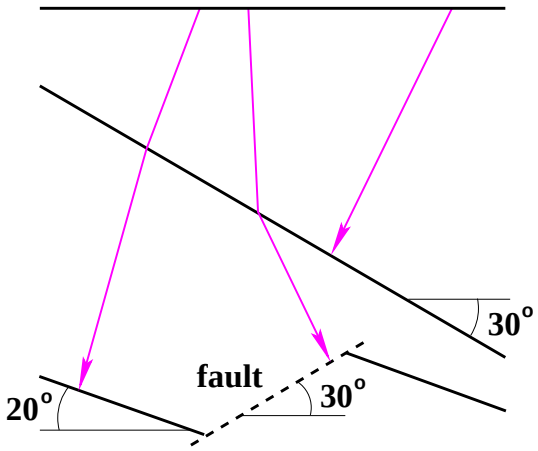

FIG. 9. The presence of fault-plane reflections in layered VTI medium might be sufficient to reconstruct the model in depth using P-wave reflection data.

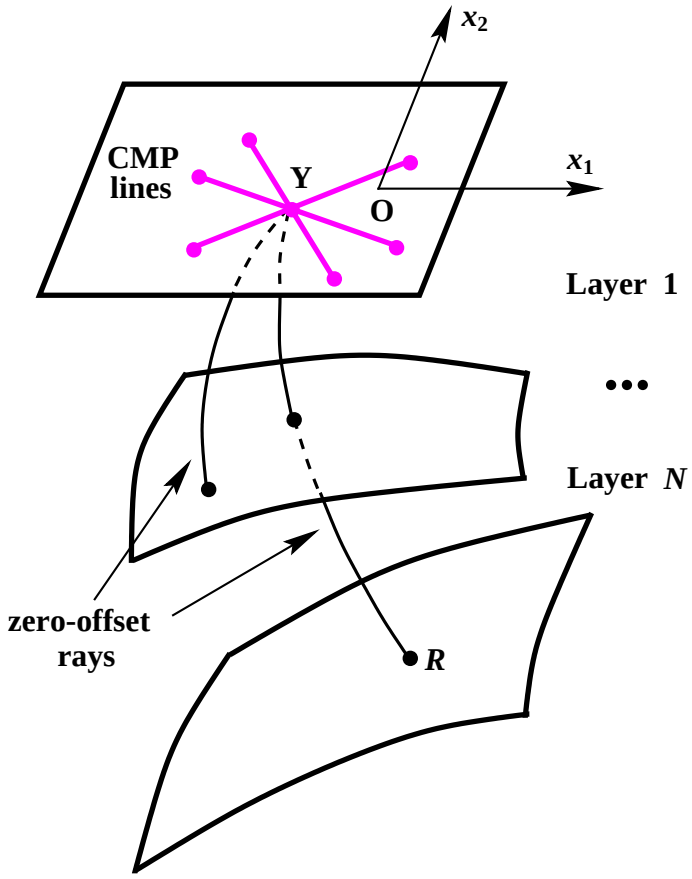

FIG. 10. Multi-azimuth CMP recording over a layered VTI model with curved interfaces.

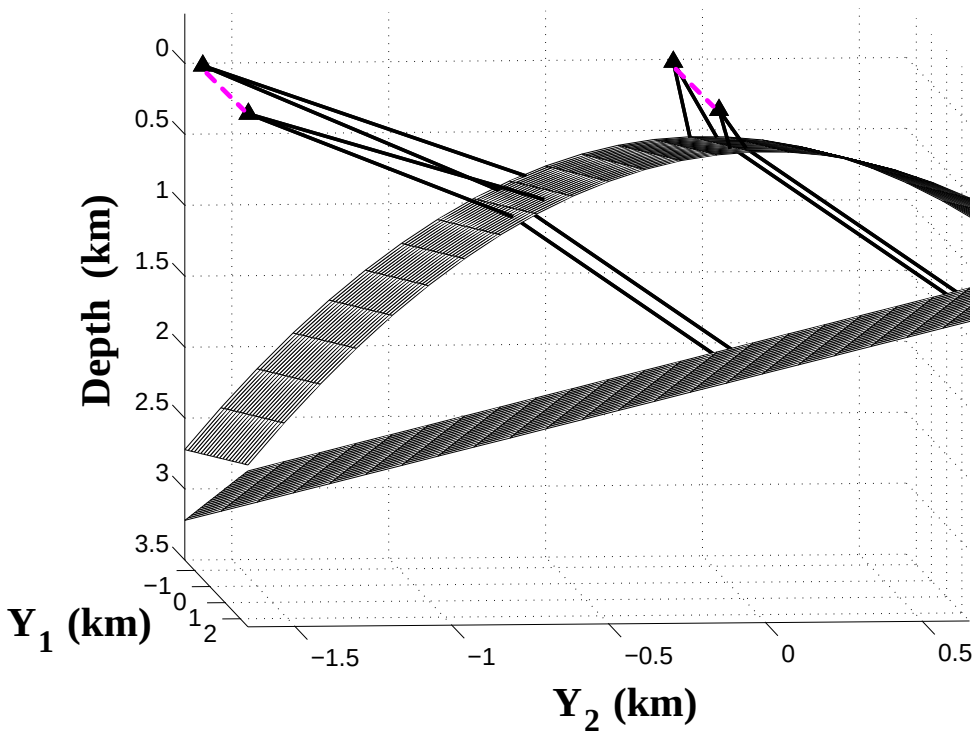

FIG. 11. Zero-offset rays in the two-layer VTI model used in the SVD analysis (Fig. 12). CMP locations are marked by triangles. The relevant interval parameters are $V_{P0,1} = 1$ km/s, $\epsilon_1 = 0.20$, $\delta_1 = 0.10$, $V_{P0,2} = 2$ km/s, $\epsilon_2 = 0.15$, $\delta_2 = 0.05$. The interfaces are described by 2-D quadratic polynomials, so $\boldsymbol{\zeta}_1$ and $\boldsymbol{\zeta}_2$ are 3×3 matrices.

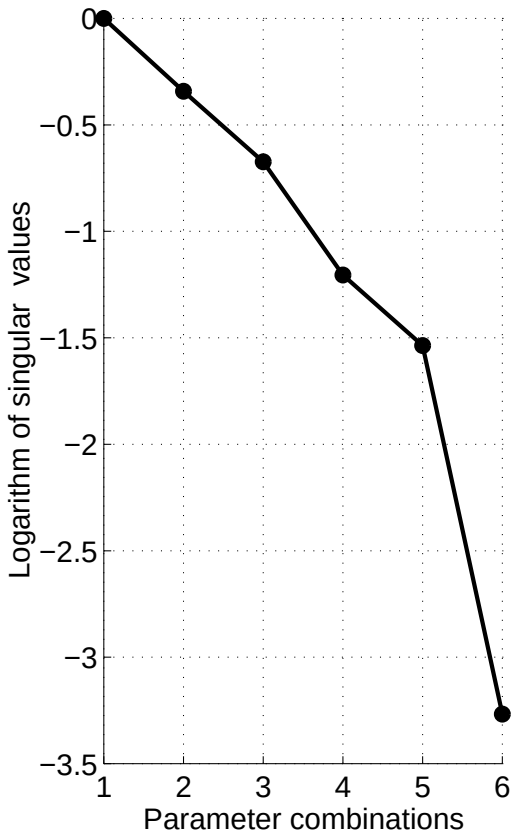

FIG. 12. Normalized singular values for the model from Fig. 11.

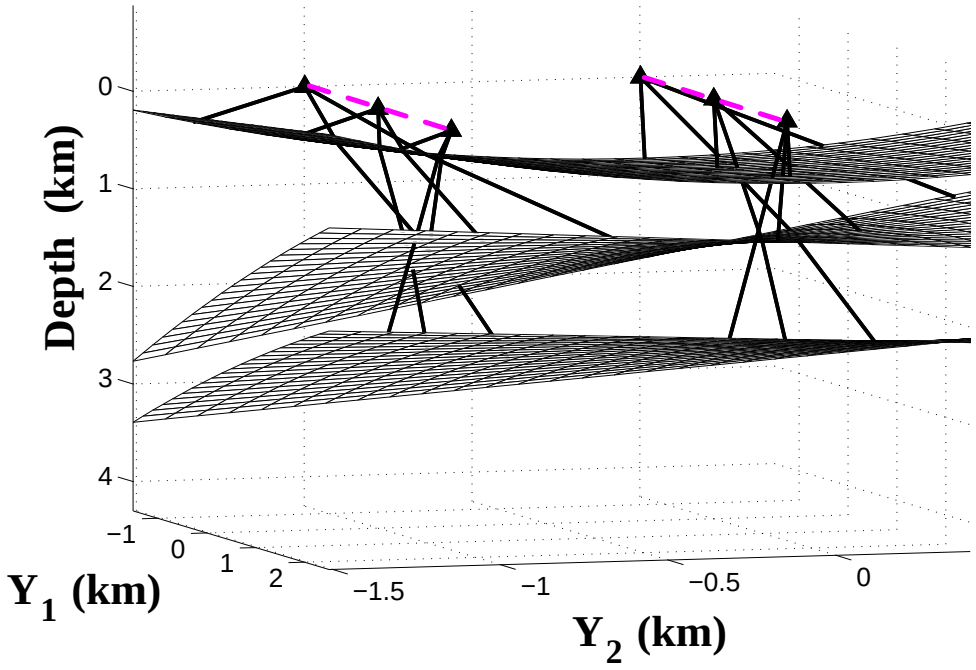

FIG. 13. Three-layer VTI model used in the inversion with several traced zero-offset rays. Common midpoints are located on the two gray dashed lines.

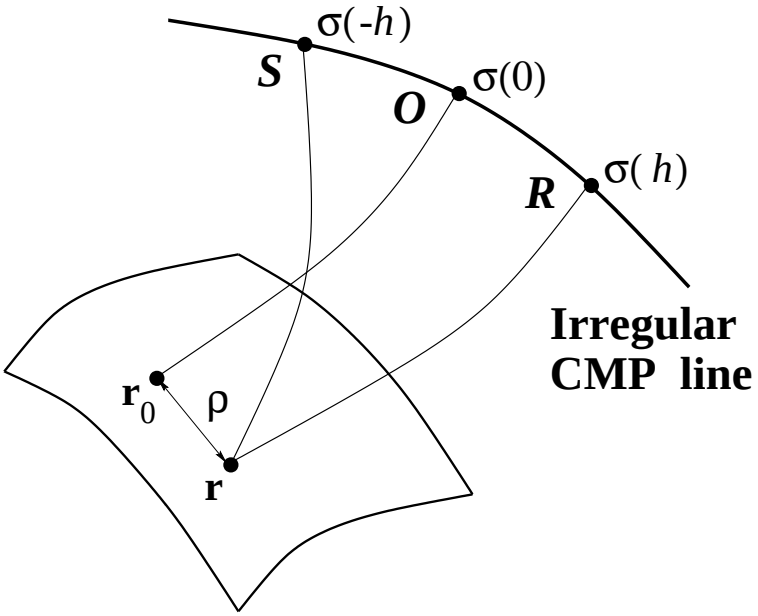

FIG. A-1. Reflection traveltimes are recorded along the curved CMP line $\boldsymbol{\sigma}$ with the common midpoint at O. Note the difference between the reflection points $\mathbf{r}_0$ and $\mathbf{r}$ of the zero-offset and nonzero-offset rays.

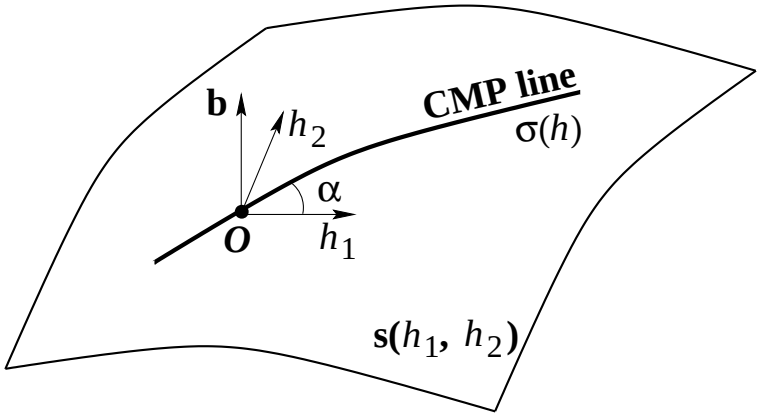

FIG. B-1. CMP line $\boldsymbol{\sigma}$ at an curved surface described by the radius-vector $\mathbf{s}(h_1, h_2)$. $\mathbf{b}$ is the unit vector orthogonal to the surface at the common midpoint O.

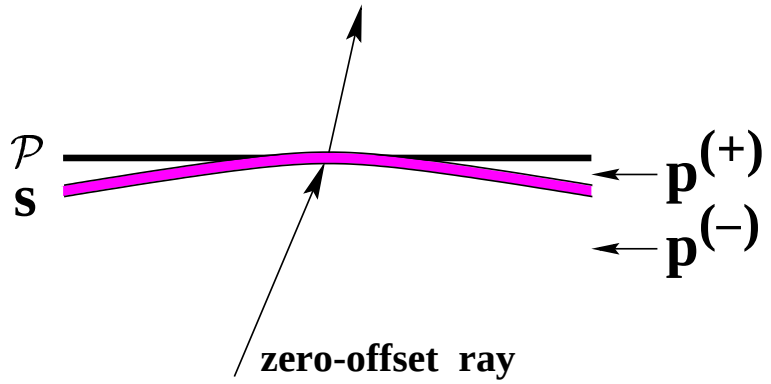

FIG. C-1. Zero-offset ray crossing a curved interface $\mathbf{s}$. Plane $\mathcal{P}$ is tangent to the interface at the intersection point; $\mathbf{p}^{(+)}$ and $\mathbf{p}^{(-)}$ are the slowness vectors on different sides of the interface.